

ISSN 0280-5316  
ISRN LUTFD2/TFRT--5779--SE

# Actuator Comparison and Coordination for Integrated Vehicle Dynamics Control

Magnus Lewander

Department of Automatic Control  
Lund University  
November 2006



<b>Department of Automatic Control</b> <b>Lund Institute of Technology</b> <b>Box 118</b> <b>SE-221 00 Lund Sweden</b>		<i>Document name</i> MASTER THESIS	
		<i>Date of issue</i> November 2006	
		<i>Document Number</i> ISRN LUTFD2/TFRT--5779--SE	
<i>Author(s)</i> Magnus Lewander		<i>Supervisor</i> Daniel Kepler at DaimlerChrysler in Sindelfingen, Germany. Karl-Erik Årzén and Brad Schofield at Automatic Control in Lund.	
		<i>Sponsoring organization</i>	
<i>Title and subtitle</i> Actuator Comparison and Coordination for Integrated Vehicle Dynamics Control (Jämförelse och koordinering av ställdon för reglering av fordonsdynamik)			
<i>Abstract</i> The purpose of this Master's Thesis was to compare and coordinate active chassis systems in a search for new ways of controlling two driving situations; <i>side wind exposure</i> and <i>split friction braking</i> . These situations were to be mastered by three active systems; active steering, brakes and suspension. Examples of how to use the systems were presented for each driving situation. The results from the investigation were then used when designing controllers for the applications. Matlab/Simulink was the key tool for evaluation of the control strategies but tests were also carried out in a real vehicle..			
<i>Keywords</i>			
<i>Classification system and/or index terms (if any)</i>			
<i>Supplementary bibliographical information</i>			
<i>ISSN and key title</i> 0280-5316			<i>ISBN</i>
<i>Language</i> English	<i>Number of pages</i> 82	<i>Recipient's notes</i>	
<i>Security classification</i>			



## Acknowledgements

This project was performed at REI/AR, DaimlerChrysler, Sindelfingen, Germany. I would like to thank Magnus Rau and Daniel Keppler for their great supervision and for giving me this interesting subject for my Master's Thesis. I am also very grateful to the other members of the team in Sindelfingen for their support whenever it was needed. Moreover, I would like to thank Prof. Karl-Erik Årzén for giving me this opportunity and my supervisor in Lund, Brad Schofield.

A handwritten signature in black ink, reading "Magnus Lewander". The signature is written in a cursive style with a long, sweeping underline that extends to the right.

Magnus Lewander



# Contents

<b>1</b>	<b>Introduction</b>	<b>4</b>
1.1	Background . . . . .	4
1.2	Purpose . . . . .	4
1.3	Method . . . . .	5
1.3.1	Software . . . . .	5
1.4	Outline . . . . .	5
1.5	Notations . . . . .	6
<b>2</b>	<b>Basics of Vehicle Dynamics</b>	<b>7</b>
2.1	Coordinate Systems . . . . .	8
2.2	Motion Variables . . . . .	8
2.3	Tire Variables . . . . .	9
<b>3</b>	<b>Active Chassis Systems</b>	<b>15</b>
3.1	Active Brakes . . . . .	15
3.1.1	Anti-lock Braking System (ABS) . . . . .	15
3.2	Active Steering . . . . .	16
3.2.1	Power Steering (PS) . . . . .	16
3.2.2	Active Front Steering (AFS) . . . . .	17
3.2.3	Steer by Wire (SBW) . . . . .	17
3.3	Active Suspension System . . . . .	18
3.3.1	Active Body Control (ABC) . . . . .	18
3.4	Electronic Stability Program (ESP) . . . . .	18
<b>4</b>	<b>Vehicle Modelling</b>	<b>20</b>
4.1	Deriving a Onetrack Model . . . . .	20
4.1.1	Stability Analysis . . . . .	22
<b>5</b>	<b>Side Wind Disturbance</b>	<b>24</b>
5.1	Introduction . . . . .	24
5.2	Side Wind Modelling . . . . .	25
5.3	Applicable Actuators to Support the Driver . . . . .	26
5.4	An Extended Onetrack Model . . . . .	28

---

5.4.1	Validation of the Onetrack Model . . . . .	31
5.5	Side Wind Estimation . . . . .	32
5.6	Feedforward Control Design . . . . .	36
5.7	Simulation Results . . . . .	37
5.7.1	Method . . . . .	37
5.7.2	Actuator Comparison . . . . .	38
5.7.3	Simultaneous Actuator Interference . . . . .	41
5.8	Results on the Test Track . . . . .	45
5.9	Discussion . . . . .	46
5.10	Conclusions . . . . .	46
<b>6</b>	<b><math>\mu</math> – <i>split</i> Braking</b>	<b>48</b>
6.1	Introduction . . . . .	48
6.2	Basics of $\mu$ – <i>split</i> braking . . . . .	49
6.3	Applicable Actuators to Support the Driver . . . . .	52
6.4	Disturbance Observer for $\mu$ – <i>split</i> braking . . . . .	53
6.5	Simulation Results . . . . .	55
6.5.1	Method . . . . .	55
6.5.2	Comparison on Snow-Asphalt . . . . .	55
6.5.3	Comparison on Ice-Asphalt . . . . .	59
6.6	Discussion . . . . .	63
6.7	Conclusions . . . . .	64
<b>7</b>	<b>Global Control Concept</b>	<b>65</b>
7.1	Concept Design . . . . .	65
7.2	Criteria . . . . .	67
<b>8</b>	<b>Outlook</b>	<b>68</b>
8.1	Conclusions . . . . .	68
8.2	Future Work . . . . .	69
<b>A</b>	<b>Control Theory</b>	<b>70</b>
A.1	Dynamical System Representation . . . . .	70
A.2	Feedforward Control . . . . .	71
A.3	Disturbance Observer . . . . .	71
A.4	Disturbance Observer with Feedforward Control . . . . .	73
A.4.1	The Closed Loop . . . . .	74



# Chapter 1

## Introduction

### 1.1 Background

A typical driving situation during winter is braking with dissimilar friction between the left and the right side of the vehicle. These circumstances may occur when braking on a road with bare ground in the middle of the road and snow along the side. The result is a disparity in brake forces between the left and the right wheels which creates a torque around centre of gravity making the car turn to the high friction side of the road. Due to the turning motion, the driver must interfere and counter steer in order to keep the stability of the vehicle. The situation can quickly become out of control if the driver does not react properly.

Another dangerous driving situation is when the vehicle is exposed to side wind. The impact from a sudden side wind pushes the car in the wind direction which is a safety as well as a comfort issue.

These situations are examples where active chassis systems are needed in order to help the driver maintain control over the vehicle, and thereby increase driving safety.

### 1.2 Purpose

Active chassis systems such as active brakes, steering, and suspension systems, are becoming more and more common in production cars. These systems have often been designed for a primary function but their purpose can be extended which opens up new possibilities for vehicle dynamics control. It is of interest to investigate which actuator that is the most suitable for

a given application as well as the possibility of actuator integration in an effort to improve the control.

The main purpose of this project is to compare and coordinate active chassis systems in a search for new ways of controlling two driving situations; Side wind exposure and  $\mu - split$  braking. These situations are to be mastered by three active systems; active steering, brakes and suspension.

## 1.3 Method

The project has been carried out at DaimlerChrysler AG, Vehicle Systems Dynamics, in Sindelfingen outside Stuttgart, Germany. The work has been structured in the following manner:

- Study vehicle dynamics, active chassis systems and control theory
- Derive a vehicle model that includes the actuators
- Investigate how the actuators can be used in the driving situations; Side wind exposure and  $\mu - split$  braking
- Derive controllers and implement them in Matlab/Simulink
- Evaluate the actuators and the control strategies in simulation
- Test the most promising systems in a test vehicle

### 1.3.1 Software

Matlab/Simulink has been used for simulation of controllers and models. The reference model of the vehicle is called CASCaDE. CASCaDE is not an ordinary dynamic system, instead it is built on characteristic curves that are tuned to fit the test vehicles behavior. It is originally modelled in Fortran but in order to run it on the Matlab/Simulink platform it has been converted to an s-function. The controllers were implemented in the test vehicle through dSpace/RapidPro.

## 1.4 Outline

**Chapter 2:** Introduces the vehicle variables that are used in this project. Focus is on the motion in the horizontal plane.

**Chapter 3:** Presents the active chassis systems that are used in this project. Each systems functions and actuators are presented.

**Chapter 4:** This chapter describes the vehicle model which the control is based on. The model is called onetrack model or bicycle model, a model which is very well known and frequently used in the automotive industry.

**Chapter 5:** In this chapter strategies to control side wind disturbances are derived. Results are presented from both simulations and a test vehicle.

**Chapter 6:** This chapter focuses on the situation when braking on a  $\mu$ -split road. Control strategies are derived and evaluated in simulation.

**Chapter 7:** In Chapter 7 a possible design of a global vehicle dynamics controller is presented. Focus is on an architecture that integrates control systems designed for different applications.

**Chapter 8:** In chapter 8 conclusions based on the results made in this thesis are presented. After that proposals for future work are stated.

## 1.5 Notations

Bold letters denote vectors or matrices. The index  $i$  refers to the wheels where  $i = 1$  means front left,  $i = 2$  front right,  $i = 3$  rear left, and  $i = 4$  rear right. The index  $j$  refers to the axles where  $j = 1$  is the front axle and  $j = 2$  is the rear axle.

## Chapter 2

# Basics of Vehicle Dynamics

In order to describe and analyze vehicle motion in a mathematical way, dynamic models of the vehicle need to be derived. Depending on the purpose of the model, different coordinate systems and motion variables are required. This chapter presents the relevant variables in this project. Focus is on lateral and longitudinal motion, the vertical forces  $F_{z,i}$ , see Figure 2.1, are therefore assumed to be known and unaffected by the motion in the horizontal plane. For an extended description of vehicle motion and alternative ways of expressing the quantities, the reader is advised to visit [1, 2, 6, 7, 8].

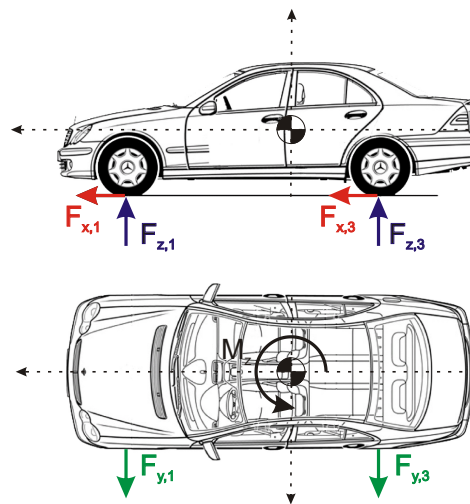


Figure 2.1: Forces acting on the car

The vehicle is treated as a rigid body that moves in a plane. It will be assumed that the body is symmetric around its longitudinal axis. The movement has then three degrees of freedom.

- Lateral direction
- Longitudinal direction
- Rotational movement around the centre of gravity

## 2.1 Coordinate Systems

As can be seen in Figure 2.2 and 2.3 three coordinate systems are used in order to describe the vehicle behaviour.

- The Earth fixed coordinate system  $(X, Y, Z)$  with its origin at some point in the environment. The vehicle driving path is described in this system.
- The Vehicle fixed coordinate system  $(x, y, z)$  has its origin in the centre of gravity. This system is used for the vehicle models.
- The Wheel fixed coordinate system  $(x_w, y_w, z_w)$  has its origin in the wheel ground contact point. The wheel forces are often calculated in this coordinate system.

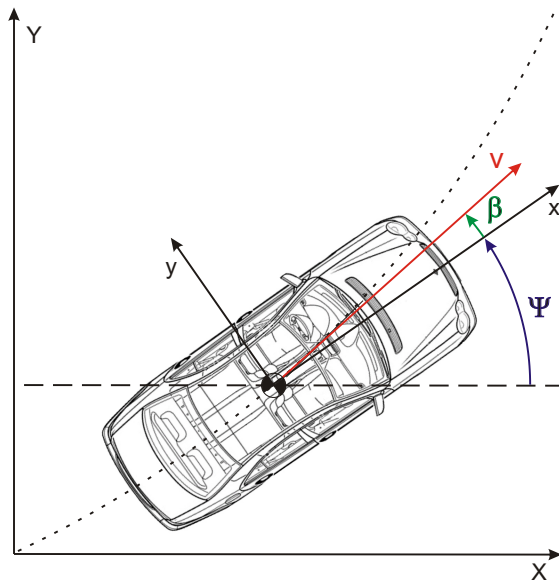


Figure 2.2: Vehicle in earth fixed coordinate system

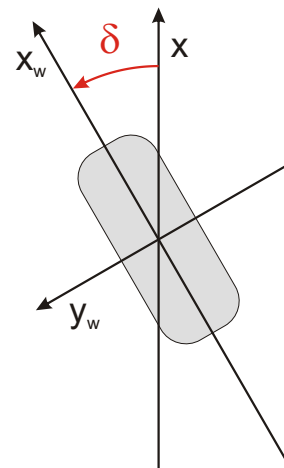


Figure 2.3: Wheel coordinate system

## 2.2 Motion Variables

### Yaw Angle

The yaw angle  $\psi$  is defined as the rotation around the vehicle vertical axis  $z$  i.e. the angle between the longitudinal axis in the vehicle fixed coordinate system and the longitudinal axis in the Earth fixed coordinate system. The time derivative of the yaw angle,  $\dot{\psi}$ , is referred to as the yaw rate. The yaw

rate is measured in the car and it is also one of the state variables when modelling a vehicle.

### Velocity and Acceleration

As can be seen in Figure 2.2, the velocity  $v$  is defined as the velocity of the center of gravity in the earth fixed coordinate system but it is often expressed in vehicle fixed coordinates. This is also the case for the acceleration  $\mathbf{a}$ . When neglecting the vertical components, the acceleration is calculated as follows:

$$\mathbf{a} = \dot{\mathbf{v}} + \boldsymbol{\omega} \times \mathbf{v} = \begin{pmatrix} \dot{v}\cos(\psi) \\ \dot{v}\sin(\psi) \\ 0 \end{pmatrix} + \begin{pmatrix} 0 \\ 0 \\ \dot{\psi} \end{pmatrix} \times \begin{pmatrix} v\cos(\psi) \\ v\sin(\psi) \\ 0 \end{pmatrix} \quad (2.1)$$

In vehicle fixed coordinates this yields:

$$a_x = \dot{v}_x - v_y\dot{\psi} \quad (2.2)$$

$$a_y = \dot{v}_y + v_x\dot{\psi} \quad (2.3)$$

### Vehicle Side Slip Angle

#### Steering Angle

The vehicle side slip angle  $\beta$  is the angle between the velocity vector acting on the center of gravity and the longitudinal axis in vehicle coordinates. This means that  $\tan(\beta) = \frac{v_y}{v_x}$ .

## 2.3 Tire Variables

The steering angle  $\delta$  is the angle between the vehicle longitudinal axis and the wheel longitudinal axis.

### Tire Side Slip Angle

The tire side slip angle  $\alpha$  is defined as the angle between the velocity vector acting on the wheel-ground contact point and the longitudinal axis in the wheel fixed coordinate

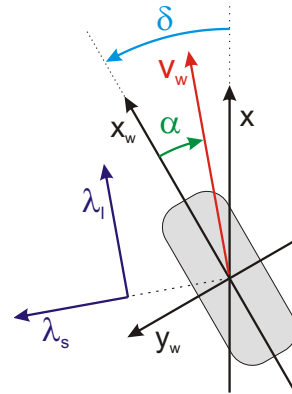


Figure 2.4:  $\alpha$ ,  $\delta$  and  $\lambda$

system. In order to include  $\alpha$  in vehicle models, an expression in vehicle fixed coordinates needs to be derived.

Figure 2.4 shows that

$$\alpha_i = \delta_i - \arctan\left(\frac{v_{w,y,i}}{v_{w,x,i}}\right) \quad (2.4)$$

Consider Figure 2.5. The velocities for each wheel are described in vehicle fixed coordinates below.

$$\begin{aligned} v_{w1} &= (v \cos(\beta) - \dot{\psi} \frac{b_f}{2}) e_x + (v \sin(\beta) + \dot{\psi} l_f) e_y \\ v_{w2} &= (v \cos(\beta) + \dot{\psi} \frac{b_f}{2}) e_x + (v \sin(\beta) + \dot{\psi} l_f) e_y \\ v_{w3} &= (v \cos(\beta) - \dot{\psi} \frac{b_r}{2}) e_x + (v \sin(\beta) - \dot{\psi} l_r) e_y \\ v_{w4} &= (v \cos(\beta) + \dot{\psi} \frac{b_r}{2}) e_x + (v \sin(\beta) - \dot{\psi} l_r) e_y \end{aligned} \quad (2.5)$$

Where  $e_x$  and  $e_y$  are the vehicle  $x$  and  $y$ -direction respectively.

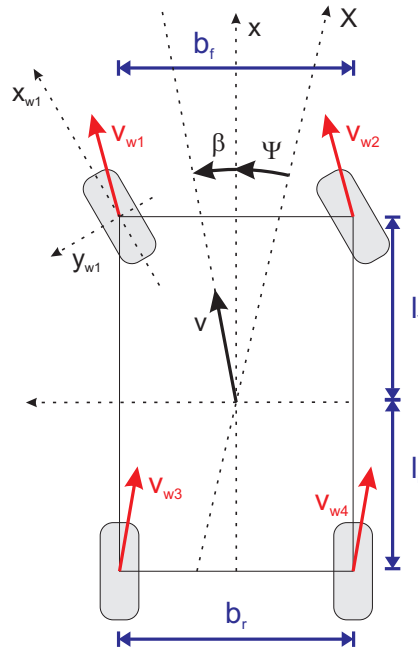


Figure 2.5: Wheel velocities

It is now possible to calculate the wheel side slip angle by inserting (2.5) into (2.4) which yields the following result.

$$\begin{aligned}
\alpha_1 &= \delta_1 - \arctan\left(\frac{v \sin(\beta) + \dot{\psi} l_f}{v \cos(\beta) - \dot{\psi} \frac{b_f}{2}}\right) \\
\alpha_2 &= \delta_2 - \arctan\left(\frac{v \sin(\beta) + \dot{\psi} l_f}{v \cos(\beta) + \dot{\psi} \frac{b_f}{2}}\right) \\
\alpha_3 &= \delta_3 - \arctan\left(\frac{v \sin(\beta) - \dot{\psi} l_r}{v \cos(\beta) - \dot{\psi} \frac{b_r}{2}}\right) \\
\alpha_4 &= \delta_4 - \arctan\left(\frac{v \sin(\beta) - \dot{\psi} l_r}{v \cos(\beta) + \dot{\psi} \frac{b_r}{2}}\right)
\end{aligned} \tag{2.6}$$

These expressions are often simplified when deriving vehicle models where small  $\beta$  and  $\alpha$  can be assumed. This simplification is described in Chapter 4.

### Wheel Slip

There are various definitions of wheel slip, in this report the Burckhardt approach is used [2]. The longitudinal slip is defined in the direction of  $v_w$ , and the lateral slip is defined in the orthogonal direction.

Tire forces build up if relative velocity occurs between the tire-road contact patch and the road surface. The ratio between the relative velocity and a given velocity is called slip  $\lambda$ . Consider Figure 2.4 and 2.6. When braking  $\lambda$  is defined as

$$\lambda_l = \frac{\omega_w r_w \cos(\alpha) - v_w}{v_w} \tag{2.7}$$

$$\lambda_s = \frac{\omega_w r_w \sin(\alpha)}{v_w} \tag{2.8}$$

and when driving it is defined as:

$$\lambda_l = \frac{\omega_w r_w \cos(\alpha) - v_w}{\omega_w r_w \cos(\alpha)} \tag{2.9}$$

$$\lambda_s = \tan(\alpha) \tag{2.10}$$

These definitions assure that the slip  $\lambda$  always is within the interval  $[-1, 1]$  where  $-1$  and  $1$  corresponds to 100% slip.

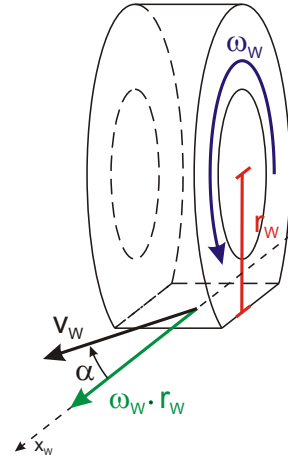


Figure 2.6: The wheel radius and angular velocity



The resulting wheel slip is the geometrical sum of the longitudinal and lateral slip.

$$\lambda = \sqrt{\lambda_l^2 + \lambda_s^2} \quad (2.11)$$

### Friction coefficient

The friction coefficient  $\mu$  is the ratio between the friction force in the horizontal plane and the wheel load.

$$\mu = \frac{F_w}{F_z} \quad (2.12)$$

One way of expressing the friction coefficient is the Burckhardt approach described below.

$$\mu(\lambda) = c_1(1 - e^{-c_2\lambda}) - c_3\lambda \quad (2.13)$$

The constants  $c_1$ ,  $c_2$  and  $c_3$  originate from the ground and tire characteristics. The corresponding lateral and longitudinal friction coefficients can be calculated as follows.

$$\mu_l = \mu \frac{\lambda_l}{\lambda} \quad \text{and} \quad \mu_s = \mu k_s \frac{\lambda_s}{\lambda} \quad (2.14)$$

### Lateral Forces

By using Equation 2.12 to 2.14, an expression for the lateral forces may be derived as follows.

The longitudinal force in the direction of  $v_w$  is

$$F_l = \mu_l F_z = \mu \frac{\lambda_l}{\lambda} F_z \quad (2.15)$$

The lateral force in the direction orthogonal to  $v_w$  is

$$F_s = \mu_s F_z = \mu k_s \frac{\lambda_s}{\lambda} F_z \quad (2.16)$$

Transformed into the wheel coordinate system the lateral force is:

$$F_{y_w} = F_s \cos(\alpha) - F_l \sin(\alpha) \quad (2.17)$$

Inserting (2.15) and (2.16) into (2.17) yields

$$F_{y_w} = \left( \mu k_s \frac{\lambda_s}{\lambda} \cos(\alpha) - \mu \frac{\lambda_l}{\lambda} \sin(\alpha) \right) F_z \quad (2.18)$$

When driving at a constant speed with small wheel side slip angles a simplified expression, derived below, can be used.

The resulting slip  $\lambda$  is, for driving, defined as follows:

$$\begin{aligned} \lambda &= \sqrt{\frac{(\omega_w r_w \cos(\alpha) - v_w)^2 + (\omega_w r_w \sin(\alpha))^2}{(\omega_w r_w)^2}} \\ &= \frac{1}{\omega_w r_w} \sqrt{(\omega_w r_w)^2 - 2\omega_w r_w v_w \cos(\alpha) + v_w^2} \end{aligned} \quad (2.19)$$

For small  $\alpha$ , the expression for  $\lambda$  becomes:

$$\lambda = \frac{1}{\omega_w r_w} \sqrt{(\omega_w r_w)^2 - 2\omega_w r_w v_w + v_w^2} = \frac{\omega_w r_w - v_w}{\omega_w r_w} = \lambda_l \quad (2.20)$$

By inserting (2.13) and (2.20) into Equation 2.18 and rewriting the wheel slip components under assumption of a small  $\alpha$ , the following expression for the lateral force is achieved.

$$F_{y_w} = \left( k_s \frac{(c_1(1 - e^{-c_2\lambda}) - c_3\lambda)}{\lambda} \right) - c_1(1 - e^{-c_2\lambda}) - c_3\lambda \alpha F_z \quad (2.21)$$

When neglecting the external forces e.g. aerodynamic drag etc.  $\lambda \approx 0$  holds. In order to calculate the limit of  $F_s$  when  $\lambda \rightarrow 0$  the second order Taylor expansion of  $e^{-c_2\lambda}$  is needed.

$$e^{-c_2\lambda} \approx 1 - c_2\lambda + \frac{c_2^2}{2}\lambda^2 \quad (2.22)$$

By inserting this into Equation 2.21 the limit is calculated as follows:

$$\begin{aligned} \lim_{\lambda \rightarrow 0} F_{y_w} &= \lim_{\lambda \rightarrow 0} \left( k_s \frac{(c_1(1 - (1 - c_2\lambda + \frac{c_2^2}{2}\lambda^2)) - c_3\lambda)}{\lambda} \right) - \\ &\quad - c_1(1 - (1 - c_2\lambda + \frac{c_2^2}{2}\lambda^2)) - c_3\lambda \alpha F_z \\ &= (k_s c_1 c_2 - c_3) \alpha F_z \end{aligned} \quad (2.23)$$

The result is a simplified expression for the side force  $F_s$  which is valid in non critical driving situations.

$$F_{y_w,i} = c_i F_{z,i} \alpha \quad (2.24)$$

The constant  $c_i$  is called cornering stiffness factor, it is adapted for each wheel since  $c_1, c_2, c_3$  and  $k_s$  are depending on road friction, tire pressure etc.

### Longitudinal Forces

Longitudinal forces are derived in a similar way as the lateral forces.

$$F_{x_w} = F_l \cos(\alpha) + F_s \sin(\alpha) \quad (2.25)$$

When inserting (2.15) and (2.16) into (2.25) the following expression is achieved.

$$F_{x_w} = \left( \mu \frac{\lambda_l}{\lambda} \cos(\alpha) - \mu k_s \frac{\lambda_s}{\lambda} \sin(\alpha) \right) F_z \quad (2.26)$$

## Chapter 3

# Active Chassis Systems

This chapter presents active systems and actuators that are used in this project.

### 3.1 Active Brakes

#### 3.1.1 Anti-lock Braking System (ABS)

The ABS is a control system which prevents the wheels from locking while braking. It has two purposes

- Help the driver to maintain steering control
- Shorten the braking distance

The shortest braking distance is reached when the wheels operate at the slip of maximum adhesion coefficient  $\mu_{l,max}$  see Figure 3.2.

A simple description of the control system in ABS is described below. For a more detailed explanation see [1, 2]. Consider Figure 3.1, the brake torque at the wheel base depends on the applied braking pressure  $p_B$  yielding.

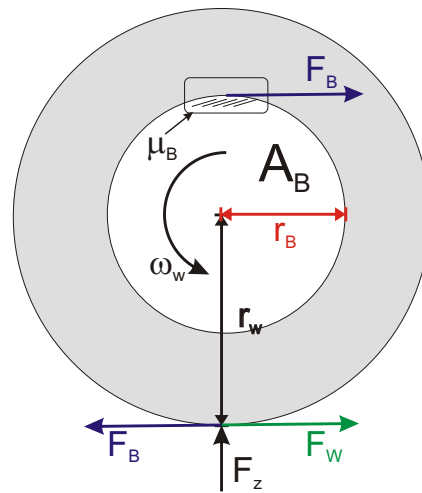


Figure 3.1: Picture of wheel with brake system

$$T_B = F_B r_w = r_B \mu_B A_B p_B = r_w k_B p_B \quad (3.1)$$

Where  $T_B$  is the brake torque,  $r_w$  is the wheel radius,  $\mu_B$  is the friction coefficient of brakes and  $A_B$  is the brake area.

The wheel torque balance, without drive torque, may now be modelled as follows.

$$J_w \dot{\omega}_w = r_w \mu_l(\lambda_l) F_z - r_w k_B p_B \quad (3.2)$$

When applying brake pressure, the difference on the right hand side of Equation 3.2 becomes negative yielding a decrease in wheel angular velocity,  $\omega$ . This means that the longitudinal wheel slip  $\lambda_l$  increases, see Section 2.3. At first the friction coefficient  $\mu_l(\lambda_l)$  increases as well

which narrows the torque difference. If  $p_B$  is continuously increasing the slip will pass the point of  $\mu_{l,max}$  and the loop becomes unstable yielding a high deceleration of the wheel rotation which causes lock-up.

In order to apply a brake pressure that gives a friction close to  $\mu_{l,max}$ , the ABS system measures  $\omega_w$  which is used to calculate the wheel equivalent speed  $v_r = \omega_w r_w$ . The differentiation  $\dot{v}_r$  is then calculated and controlled with brake pressure so that it is kept within a region which gives high friction.

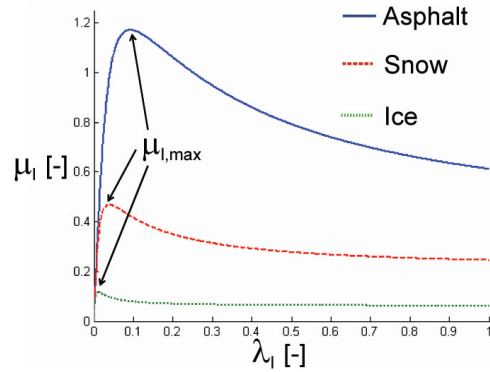


Figure 3.2:  $\mu_l$  versus  $\lambda_l$  when  $\alpha = 0$

## 3.2 Active Steering

There are different kinds of active steering systems. In this project an arbitrary steering system, modelled with a linear relation between the steering wheel angle  $\delta_{sw}$  and the steering angle  $\delta$ , is used. This means that the outputs from the controllers in simulation will be treated as steering wheel angles. The reason for this approach is that the controllers developed in this project deliver set points for the actuators. This means that several systems might be suitable as long as they are fast and accurate. Some of the active steering systems are presented below.

### 3.2.1 Power Steering (PS)

Power steering is a well known system that is mounted in almost every new car. Its main purpose is to reduce the steering effort by adding a torque at

the steering rod. There are currently three kinds of power steering; Hydraulic (HPS), Electric (EPS) and Electro-hydraulic (EHPS). The hydraulic power steering is mechanical and driven by the vehicle engine while the electric is driven by an independent electric motor where the intervention is calculated by a computer. The electro-hydraulic system consists of an electric motor that provides hydraulic pressure, the applied torque is calculated by a computer.

It is possible, by modifying the software for EPS and EHPS, to add torque on the steering rod even when the driver does not steer. These systems may then be used for active steering where the applied steering angle is based on commands given by other systems e.g. a yaw rate controller.

### 3.2.2 Active Front Steering (AFS)

The Active Front Steering is a steering system with variable transmission ratios and power assistance. An electromechanical actuator between the steering wheel and the steering transmission adds an additional positive or negative steering angle to the input applied by the driver. It uses a planetary gear with two input shafts and one output shaft flanged onto the rack and pinion steering gear. One of the input shafts is connected to the steering wheel, the second is driven by an electric motor. The overall steering angle applied on the output shaft is made up of the steering wheel angle plus the angle of the electromechanical adjuster.

### 3.2.3 Steer by Wire (SBW)

A steer by wire system does not have any mechanical connection between the steering wheel and the wheels. Instead it uses electric motors which get instructions from a computer that calculates the desired steering angle from the steering wheel action. The advantage by using this solution is that an additional steering angle can be applied without the driver feeling anything. This is convenient when large steering angles are demanded for skid prevention etc. However, since the vehicle becomes uncontrollable in terms of steering if the system shuts down, this is not used in production cars.

### 3.3 Active Suspension System

#### 3.3.1 Active Body Control (ABC)

The active suspension system used in this project is the Active Body Control suspension found in some of Mercedes-Benz production cars. The purpose of the ABC system is to enhance the driver comfort and to decrease the vehicle roll angle during cornering. The system consists of a steel spring, a damper and a hydraulic cylinder. Through the hydraulics, a change in wheel load can be made by changing the position of the spring. The system is unique for DaimlerChrysler and in order to get more information about it read [10]. By modifying the ABC system a permanent change in wheel loads can be applied, see Figure 3.3. This is called warp and it is in this project defined as follows.

$$w = F_{z,1} - F_{z,2} - F_{z,3} + F_{z,4} \quad (3.3)$$

The torque equilibrium around the lateral and longitudinal axis remain unchanged which means that no pitch or roll motion is induced by this manoeuvre. This means that when warp is positive the left front and the right rear wheel have more wheel load than the other two wheels.

The maximum amount of warp is limited either by the suspension construction which can be saturated or by the physical limit  $\max(|w|) \leq 4 \cdot \min(F_{z,i})$  which means that the largest force that can be translated from a wheel can not be larger than the original wheel load.

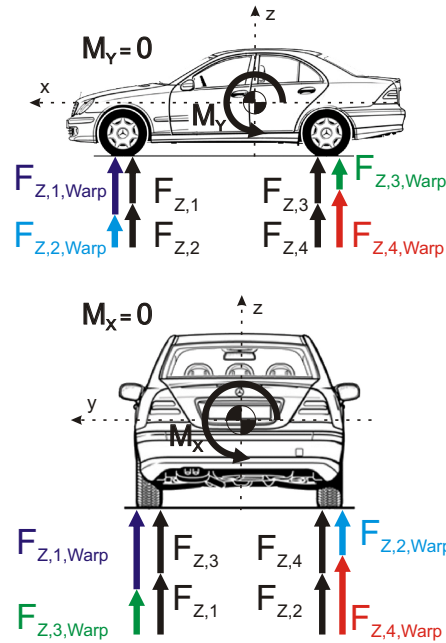


Figure 3.3: Force equilibrium during warp

### 3.4 Electronic Stability Program (ESP)

An ESP system's basic function is more or less a yaw rate and lateral acceleration controller that acts as supervisor to the active brakes. It compares

the driver's intended direction in steering and braking inputs, to the vehicle's response, via lateral acceleration, rotation and individual wheel speeds. ESP then brakes individual front or rear wheels and, in some configurations, reduces excess engine power as needed to help correct under steering or over steering. Future ESP systems will include additional actuators such as active steering and suspension in order to improve the performance. This might, however, go under another name.



# Chapter 4

## Vehicle Modelling

Process models are vital for behavior analysis and control design. In the case of vehicle modelling, several models have been derived for a number of purposes. In general a simple model is preferable as long as its performance coincides with the process'. This chapter focuses on such a model, the onetrack model found in [8].

### 4.1 Deriving a Onetrack Model

The idea of a onetrack model, see Figure 4.1, also known as bicycle model, is to simplify the dynamics of the vehicle but maintain the behaviour. It is valid when driving at a constant speed and manoeuvring with moderate steering angles and low slip.

The onetrack model used in this project is a second order dynamical system. The approach uses the yaw rate  $\dot{\psi}$  and the time derivative of the lateral velocity  $\dot{v}_y$  as state variables.

Newton's second law is applied to the chassis yielding the following equations.

Force equilibrium in the longitudinal direction

$$ma_y = F_{y,f} \cos(\delta) + F_{y,r} \quad (4.1)$$

Torque equilibrium around the altitude axis

$$J_z \ddot{\psi} = l_f F_{y,f} \cos(\delta) - l_r F_{y,r} \quad (4.2)$$

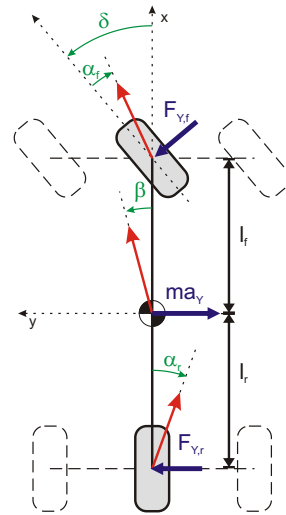


Figure 4.1: The idea behind the onetrack model

These equations can be linearised under the assumption that only small angles will be used e.g.  $\delta, \alpha, \beta < 10^\circ$ . This means that  $\cos(\delta) \approx 1$  and  $\beta = \frac{v_y}{v_x}$ . This gives the following dynamical system:

$$J_z \ddot{\psi} = l_f F_{y,f} - l_r F_{y,r} \quad (4.3)$$

$$\dot{v}_y = -v_x \dot{\psi} + \frac{1}{m} (F_{y,f} + F_{y,r}) \quad (4.4)$$

As previously mentioned in Section 2.3, with small  $\alpha$  and  $\lambda$  the lateral forces can be described by a constant originating from the tire adhesion characteristics multiplied with the tire side slip angle  $\alpha$  and the wheel load  $F_z$ .

$$F_{y,f} = c_f F_{z,f} \alpha_f \quad (4.5)$$

$$F_{y,r} = c_r F_{z,r} \alpha_r \quad (4.6)$$

Additionally, if the wheel load is assumed constant, the expressions for the front and rear tire forces are.

$$F_{y,f} = C_f \alpha_f \quad (4.7)$$

$$F_{y,r} = C_r \alpha_r \quad (4.8)$$

Consider Equation 2.6. The expression for  $\alpha$  can, under the assumption that  $\beta$  is small and that  $b_f = b_r = 0$  which directly follows from the onetrack approach, be described as:

$$\alpha_f = \delta - \frac{v_y + l_f \dot{\psi}}{v_x} \quad (4.9)$$

$$\alpha_r = -\frac{v_y}{v_x} + \frac{l_r \dot{\psi}}{v_x} \quad (4.10)$$

By inserting (4.7)-(4.10) into (4.3) and (4.4) a state space representation is obtained.

$$\begin{pmatrix} \ddot{\psi} \\ \dot{v}_y \end{pmatrix} = \begin{pmatrix} -\frac{l_f^2 C_f + l_r^2 C_r}{J_z v_x} & \frac{l_r C_r - l_f C_f}{-C_f + C_r} \\ -v_x + \frac{l_r C_r - l_f C_f}{m v_x} & -\frac{J_z v_x}{m v_x} \end{pmatrix} \begin{pmatrix} \dot{\psi} \\ v_y \end{pmatrix} + \begin{pmatrix} \frac{l_f C_f}{J_z} \\ \frac{C_f}{m} \end{pmatrix} \delta \quad (4.11)$$

The system matrix  $\mathbf{A}$  is time invariant under the condition that  $\dot{v}_x = 0$ .

#### 4.1.1 Stability Analysis

The system poles which also are the eigenvalues to  $\mathbf{A}$ , are calculated to analyze the stability of the system. They are obtained by solving (4.12).

$$\begin{aligned} \det(s\mathbf{I} - \mathbf{A}) &= 0 \\ s^2 + \left(\frac{\sigma}{mv_x} + \frac{\kappa}{J_z v_x}\right) s + \left(\frac{\kappa\sigma - \rho^2}{mJ_z v_x^2} + \frac{\rho}{J_z}\right) &= 0 \end{aligned} \quad (4.12)$$

Which gives:

$$s_{1,2} = -\frac{1}{2} \left(\frac{\sigma}{mv_x} + \frac{\kappa}{J_z v_x}\right) \pm \sqrt{\frac{1}{4} \left(\frac{\sigma}{mv_x} + \frac{\kappa}{J_z v_x}\right)^2 - \left(\frac{\kappa\sigma - \rho^2}{mJ_z v_x^2} + \frac{\rho}{J_z}\right)} \quad (4.13)$$

The system is stable except when

$$\frac{1}{2} \left(\frac{\sigma}{mv_x} + \frac{\kappa}{J_z v_x}\right) < \sqrt{\frac{1}{4} \left(\frac{\sigma}{mv_x} + \frac{\kappa}{J_z v_x}\right)^2 - \left(\frac{\kappa\sigma - \rho^2}{mJ_z v_x^2} + \frac{\rho}{J_z}\right)} \quad (4.14)$$

which can be simplified to

$$C_f C_r (L)^2 < -mv_x^2 (l_r C_r - l_f C_f) \quad (4.15)$$

where the left part of the equation is positive. Since  $m$  is the mass of the vehicle and  $v_x$  has a real value this means that  $l_r C_r - l_f C_f < 0$  which corresponds to a vehicle with over steering characteristics.

Figure 4.2 shows a pole diagram for lateral velocities between 20 km/h to 180 km/h. With the model parameters taken from the test vehicle the poles become complex for  $v_x > 22.3$  km/h.

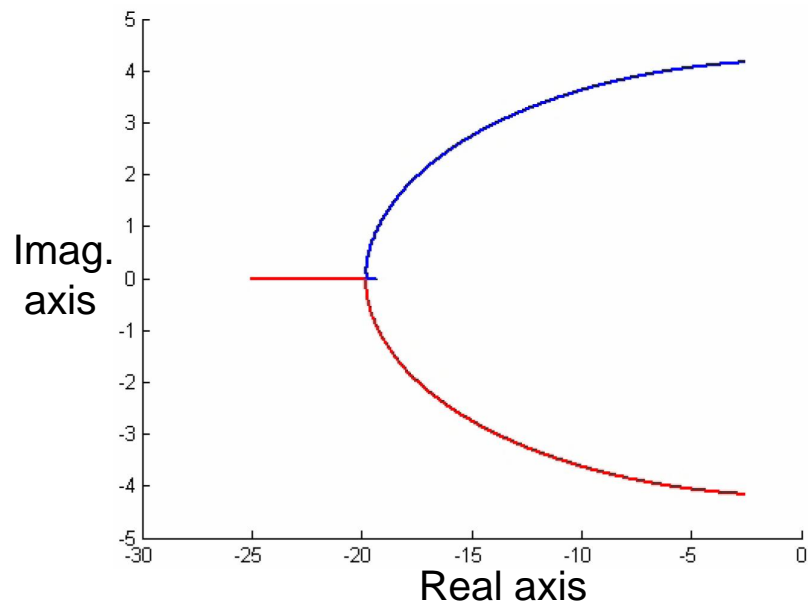


Figure 4.2: Pole diagram for the onetrack model

## Chapter 5

# Side Wind Disturbance

### 5.1 Introduction

Side wind interference is a well known disturbance among drivers. The impact from a sudden side wind pushes the car in the wind direction which is a safety issue as well as a comfort issue. Most of today's production cars do not have any system that counteracts the wind force. It is of interest to find a solution to measure or estimate the wind and then use the information to compensate the wind force. It would be preferable to control side wind with existing actuators and sensors. In the following chapter an approach to estimating side wind, using a disturbance observer, is presented. Furthermore feedforward controllers are designed for the active chassis systems in an attempt to keep the influence of side wind at a low level.

## 5.2 Side Wind Modelling

In order to estimate side wind, a model of the wind force applicable to the onetrack model is derived. The idea of how to model it is taken from [3]. Figure 5.1 shows the wind flow direction when side wind is present. The component in the  $x$ -direction is caused by the vehicle velocity and the component in the  $y$ -direction is the side wind. By calculating the geometrical sum of these wind components a resultant wind flow  $v_{res,wind}$  is obtained.

$$v_{res,wind} = \sqrt{v_{x,wind}^2 + v_{y,wind}^2} \quad (5.1)$$

$$\tau_{wind} = \arctan\left(\frac{v_{y,wind}}{v_{x,wind}}\right) \quad (5.2)$$

The wind flow causes a force in the lateral direction and a torque around the centre of the vehicle which can be expressed as follows:

$$S_w = \frac{\rho_w}{2} c_s(\tau_w) A_s v_{res,wind}^2 \quad (5.3)$$

$$M_z^* = \frac{\rho_w}{2} c_N(\tau_w) A_s v_{res,wind}^2 L \quad (5.4)$$

where  $\rho_w$  is the density of the air,  $A_s$  is the area of the vehicle's front and  $c_s(\tau_w)$  and  $c_N(\tau_w)$  are air resistance coefficients originating from the vehicle hull properties.

The torque  $M_z^*$  needs to be translated to the centre of gravity in order to be used in a onetrack model. This is done in the approach below:

$$M_z = S_w e \quad (5.5)$$

where  $e = \frac{c_N^*}{c_s^*} L$  and  $c_N^* = \left(c_N + c_s \left(\frac{l_f}{L} - \frac{1}{2}\right)\right)$ . For small  $\tau_w$  it is assumed that  $e$  is constant.

It is now possible to include the side wind force in the onetrack model, which is done in Section 5.4.

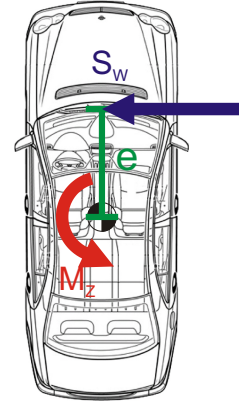
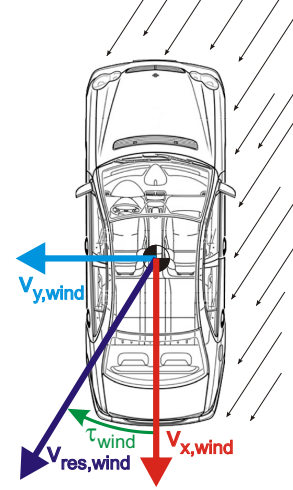


Figure 5.1: Wind velocities and force model

## 5.3 Applicable Actuators to Support the Driver

### Active Steering

When a vehicle is exposed to side wind, the driver counter steers with the steering wheel. With an active steering system the same manoeuvre can be carried out automatically with shorter reaction time and higher precision as a result.

### Brake Steering

Another way of controlling the direction in which the vehicle is heading is obtained by dissimilar braking. This technology is already implemented in ESP systems which have been on the market for a couple of years. If a vehicle is equipped with a brake system that allows the brake pressure  $p_B$  to be distributed to each wheel independently, it is possible to steer the vehicle by applying brake forces in a way that creates a torque around the vertical axis as described below:

$$J_z z \ddot{\psi} = (F_{y,1} + F_{y,2})l_f - (F_{y,3} + F_{y,4})l_r + (F_{x,2} - F_{x,1})\frac{b_f}{2} + (F_{x,4} - F_{x,3})\frac{b_r}{2} \quad (5.6)$$

Due to the construction of the suspension system there are further effects that need to be taken into account. The brake forces applied have an effect on the steering angle  $\delta_i$ . The effect can be approximated as proportional to the difference in brake force between the left and the right side of the vehicle yielding the following expression for the steering angle:

$$\delta_i = \delta_{0,i} + k_{\Delta F_{x,j}}(F_{l,2} - F_{l,1} + F_{l,4} - F_{l,3}) \quad (5.7)$$

where  $i$  and  $j$  are the wheel and axle indices respectively. In Figure 5.2

the steering angle changes are shown in three cases with different brake forces applied. The results show an almost linear dependency between brake force and steering angle.

The steering effect is different depending on what wheel or wheels that brake. Assuming that the car is symmetric over the longitudinal axis  $x$  it sufficient to brake the wheels on one side of the vehicle in order to show the effect. Three

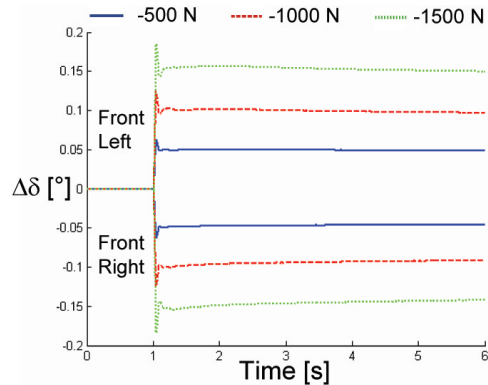


Figure 5.2: Steering angle change for different brake forces applied at the front axle

cases need to be compared; braking the front wheel, rear wheel and front and rear wheel simultaneously. In order to decide which method to choose, simulations were carried out comparing the alternatives. The total brake force was the same in all simulations. The yaw rate was used as a measurement of vehicle steering. The result is displayed in Figure 5.3.

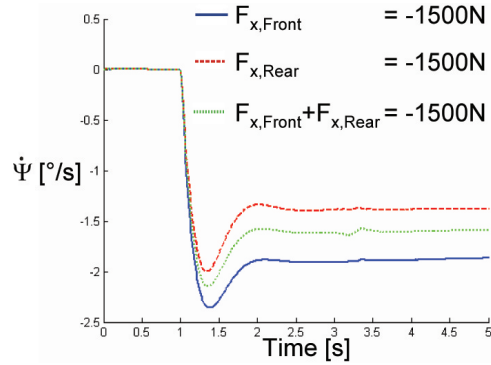


Figure 5.3: Responses in  $\dot{\psi}$  when braking with a total brake force of -1500 N

It can be seen that braking on the front wheel gives the highest yaw rate for a given brake force, moreover, since the car is rear wheel driven, brake torque added at the rear axle will interfere with the drive torque from the engine. Due to the results, front wheel brake steering will be used in this project.

### Suspension Steering

The Active Body Control system can apply warp which can be used in this application since it has, under normal driving conditions, an effect on the steering angle [9].

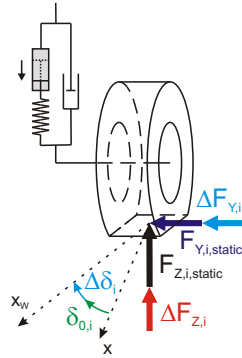


Figure 5.4: Steering angle change

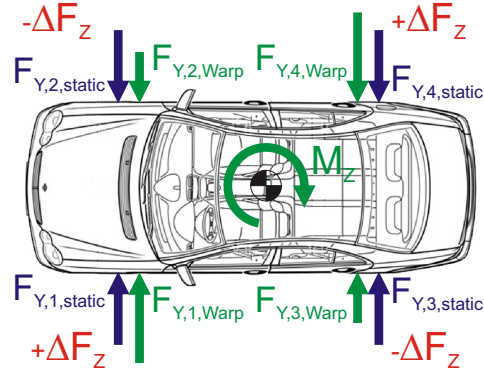


Figure 5.5: Force change

By changing the wheel loads a change in steering angle is achieved which is illustrated in Figure 5.4 and 5.5. This means that ABC can be used to create a torque around the altitude axis which counter acts the motion induced by wind. The change in steering angle is modelled as follows:

$$\delta_i = \delta_{0,i} + k_{w,j} \cdot \frac{Fz,j,r - Fz,j,l}{Fz,j,r + Fz,j,l} \quad (5.8)$$



## 5.4 An Extended Onetrack Model

In the previous section two additional steering approaches were introduced. These steering systems and the side wind force are included in an extended onetrack model below.

The motion equations are once again presented, this time including the wind force and a longitudinal force component.

$$J_{\psi} \ddot{\psi} = l_f(F_{y,1}F_{y,2}) - l_r(F_{y,3} + F_{y,4}) + \frac{b_f}{2}(\Delta F_x) + S_w e \quad (5.9)$$

$$\dot{v}_y = -v_x \dot{\psi} + \frac{1}{m}(F_{y,1} + F_{y,2} + F_{y,3} + F_{y,4}) + \frac{S_w}{m} \quad (5.10)$$

The forces  $F_{y,i}$  are modelled as a function of side slip angle, tire stiffness and wheel load:

$$F_{y,i} = c_i F_{z,i} \alpha_i \quad (5.11)$$

The wheel load distribution when the vehicle is standing still ( $\dot{v} = v = 0$ ) is calculated, by using the torque equilibrium around the longitudinal and lateral axis, to become:

$$\begin{aligned} F_{z,1}^* &= \frac{mgl_r}{2(l_f+l_r)} \\ F_{z,2}^* &= \frac{mgl_r}{2(l_f+l_r)} \\ F_{z,3}^* &= \frac{mgl_f}{2(l_f+l_r)} \\ F_{z,4}^* &= \frac{mgl_f}{2(l_f+l_r)} \end{aligned} \quad (5.12)$$

The definition of warp is once again presented

$$w = F_{z,1} - F_{z,2} - F_{z,3} + F_{z,4} \quad (5.13)$$

Warp is distributed over the four wheels in accordance with the torque and force equilibrium. Together with Equation 5.12, this yields an extended description of the stationary wheel loads.

$$\begin{aligned} F_{z,1} &= \frac{mgl_r}{2(l_f+l_r)} + \frac{w}{4} \\ F_{z,2} &= \frac{mgl_r}{2(l_f+l_r)} - \frac{w}{4} \\ F_{z,3} &= \frac{mgl_f}{2(l_f+l_r)} - \frac{w}{4} \\ F_{z,4} &= \frac{mgl_f}{2(l_f+l_r)} + \frac{w}{4} \end{aligned} \quad (5.14)$$

The applied warp and the difference in longitudinal forces affect the steer angle as described in the expression below:

$$\Delta\delta_j = \pm\delta_{j,0} + k_{w,f} \cdot \frac{F_{z,j,r} - F_{z,j,l}}{F_{z,j,r} + F_{z,j,l}} + k_{\Delta F_{x,j}} \cdot (F_{x,r} - F_{x,l}) \quad (5.15)$$

This term will change the expression for  $\alpha$ . Superposed to the vehicle side slip angles defined in Equation 4.9 and 4.10 the new expression yields:

$$\alpha_1 = \delta - \frac{v_y + l_f \dot{\psi}}{v_x} - \delta_{f,0} + k_{w,f} \cdot \frac{F_{z,2} - F_{z,1}}{F_{z,2} + F_{z,1}} + k_{\Delta F_{x,f}} \cdot \Delta F_x \quad (5.16)$$

$$\alpha_2 = \delta - \frac{v_y + l_f \dot{\psi}}{v_x} + \delta_{f,0} + k_{w,f} \cdot \frac{F_{z,2} - F_{z,1}}{F_{z,2} + F_{z,1}} + k_{\Delta F_{x,f}} \cdot \Delta F_x \quad (5.17)$$

$$\alpha_3 = -\frac{v_y - l_r \dot{\psi}}{v_x} - \delta_{r,0} + k_{w,r} \cdot \frac{F_{z,4} - F_{z,3}}{F_{z,4} + F_{z,3}} + k_{\Delta F_{x,r}} \cdot \Delta F_x \quad (5.18)$$

$$\alpha_4 = -\frac{v_y - l_f \dot{\psi}}{v_x} + \delta_{r,0} + k_{w,r} \cdot \frac{F_{z,4} - F_{z,3}}{F_{z,4} + F_{z,3}} + k_{\Delta F_{x,r}} \cdot \Delta F_x \quad (5.19)$$

By using the Equations from 5.9 to 5.19 the extended motion equations can be derived:

$$\begin{aligned} \ddot{\psi} = & \frac{1}{J_z} (l_f C_f (\delta - \frac{v_y + l_f \dot{\psi}}{v_x} + k_{\Delta F_{x,f}} \Delta F_x) - l_r C_r (-\frac{v_y - l_f \dot{\psi}}{v_x} + k_{\Delta F_{x,r}} \Delta F_x)) - \\ & - \frac{w}{2J_z} (l_f c_f (\delta_{0,r} + k_{w,f}) + l_r c_r (\delta_{0,r} + k_{w,r})) + \frac{b_f}{2J_z} \Delta F_x + \frac{S_{we}}{J_z} \end{aligned} \quad (5.20)$$

$$\begin{aligned} \dot{v}_y = & -v_x \dot{\psi} \frac{1}{m} (C_f (\delta - \frac{v_y + l_f \dot{\psi}}{v_x} + k_{\Delta F_{x,f}} \Delta F_x) + C_r (-\frac{v_y - l_f \dot{\psi}}{v_x} + k_{\Delta F_{x,r}} \Delta F_x)) - \\ & - \frac{w}{2m} (c_f (\delta_{0,r} + k_{w,f}) - c_r (\delta_{0,r} + k_{w,r})) + \frac{S_w}{m} \end{aligned} \quad (5.21)$$

Some constants are introduced to simplify the expressions:

$$\rho = l_r C_r - l_f C_f \quad (5.22)$$

$$\sigma = C_f + C_r \quad (5.23)$$

$$\kappa = l_r^2 C_r + l_f^2 C_f \quad (5.24)$$

$$\xi_1 = l_f c_f (\delta_{f,0} + k_{w,f}) + l_r c_r (\delta_{r,0} + k_{w,r}) \quad (5.25)$$

$$\xi_2 = c_f (\delta_{f,0} + k_{w,f}) - c_r (\delta_{r,0} + k_{w,r}) \quad (5.26)$$

$$\xi_3 = l_f C_f k_{\Delta F_{x,f}} - l_r C_r k_{\Delta F_{x,r}} + \frac{b_f}{2} \quad (5.27)$$

$$\xi_4 = C_f k_{\Delta F_{x,f}} + C_r k_{\Delta F_{x,r}} \quad (5.28)$$

Inserted in (5.20) and (5.21) this gives the new equations:

$$\ddot{\psi} = \frac{1}{J_z} \left( -\frac{\kappa}{v_x} \dot{\psi} + \frac{\rho}{v_x} v_y + l_f C_f \delta - \xi_1 w + \xi_3 \Delta F_x + S_w e \right) \quad (5.29)$$

$$\dot{v}_y = \frac{1}{m} \left( (-v_x m + \frac{\rho}{v_x}) \dot{\psi} - \frac{\sigma}{v_x} v_y + C_f \delta - \frac{\xi_2}{2} w + \xi_4 \Delta F_x + S_w \right) \quad (5.30)$$

Which can be rewritten in state space form as:

$$\begin{pmatrix} \ddot{\psi} \\ \dot{v}_y \end{pmatrix} = \begin{pmatrix} -\frac{\kappa}{J_z v_x} & \frac{\rho}{J_z v_x} \\ -v_x + \frac{\rho}{m v_x} & -\frac{\sigma}{m v_x} \end{pmatrix} \begin{pmatrix} \dot{\psi} \\ v_y \end{pmatrix} + \begin{pmatrix} \frac{l_f C_f}{J_z} & \frac{\xi_3}{J_z} & -\frac{\xi_1}{2 J_z} & \frac{e}{J_z} \\ \frac{C_f}{m} & \frac{\xi_4}{m} & -\frac{\xi_2}{2 m} & \frac{1}{m} \end{pmatrix} \begin{pmatrix} \delta \\ \Delta F_x \\ w \\ S_w \end{pmatrix} \quad (5.31)$$

This corresponds to:

$$\dot{\mathbf{x}} = \mathbf{Ax} + \mathbf{Bu} \quad (5.32)$$

### 5.4.1 Validation of the Onetrack Model

In order to decide if the extended onetrack model is a valid vehicle model a comparison was made with the test vehicle. The model was fed with measured control signals and the model output was compared to the corresponding vehicle output. In addition were the actuators step responses tested to show the performance of the active systems. It is of highest importance that the actuators are fast and accurate since the controllers in this project deliver set point signals that are assumed to be realized immediately. In Figure 5.6 the behaviour of the onetrack model is displayed together with

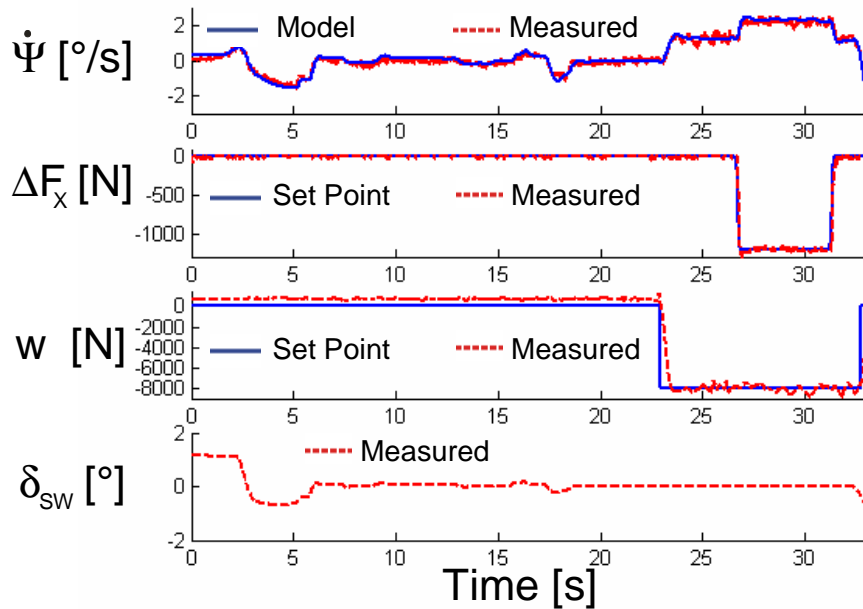


Figure 5.6: Validation of the extended onetrack model and the actuators

measurements in the actual test vehicle. Brake steering interventions are shown in the second plot, suspension steering in the third plot and steering wheel action in the fourth. It can be seen that the model output  $\dot{\psi}$  follows the measured signal during manoeuvres that include all actuators. The conclusion is that the model is suitable for the application. The measured brake force is calculated from pressure measurements with a linear dependency. The step response is very fast and accurate. When studying the step response for the suspension it can be seen that the actuator is slower than the brakes but it still reaches its set point and holds it without stationary errors.

## 5.5 Side Wind Estimation

In this section, a disturbance observer, see Appendix A, for side wind estimation is derived. In Section 5.4, a one track model consisting of both longitudinal and lateral forces was derived. That model will be the fundament to construct a disturbance observer that can be used for side wind estimation. The estimated disturbance will then be the input to steering, brake and warp controllers.

Inserting (5.14)-(5.19) into (5.11) using  $F_{y,j} = F_{y,j,r} + F_{y,j,l}$  gives:

$$F_{y,f} = C_f \left( \delta - \frac{v_y + l_f \cdot \dot{\psi}}{v_x} + k_{\Delta F_{x,f}} \Delta F_x \right) - \frac{w}{2} c_f (\delta_{f,0} + k_{w,f}) \quad (5.33)$$

$$F_{y,r} = C_r \left( -\frac{v_y - l_r \cdot \dot{\psi}}{v_x} + k_{\Delta F_{x,r}} \Delta F_x \right) + \frac{w}{2} c_r (\delta_{r,0} + k_{w,r}) \quad (5.34)$$

Introducing a force  $S_w$  originating from side wind, the following lateral force equilibrium and torque equilibrium are achieved:

$$ma_y = F_{y,f} + F_{y,r} + S_w \quad (5.35)$$

$$J_z \ddot{\psi} = l_f F_{y,f} - l_h F_{y,r} + e S_w + \frac{s_f}{2} \Delta F_{x,f} \quad (5.36)$$

Equation 5.35 can be rewritten into:

$$F_{y,f} = ma_y - F_{y,r} - S_w \quad (5.37)$$

The next step is to put Equation 5.37 into 5.36. This yields the following expression:

$$J_z \ddot{\psi} = l_f ma_y - (l_v + l_h) F_{y,r} + (e - l_f) S_w + \frac{b_f}{2} \Delta F_{x,f} \quad (5.38)$$

Then put (5.37) equal to (5.33) and insert (5.34).

$$\begin{aligned} ma_y - \left( C_r \left( -\frac{v_y - l_r \cdot \dot{\psi}}{v_x} + k_{\Delta F_{x,r}} \Delta F_x \right) + \frac{w}{2} c_r (\delta_{r,0} + k_{w,r}) \right) - S_w = \\ = C_f \left( \delta - \frac{v_y + l_f \cdot \dot{\psi}}{v_x} + k_{\Delta F_{x,f}} \Delta F_x \right) - \frac{w}{2} c_f (\delta_{f,0} + k_{w,f}) \end{aligned} \quad (5.39)$$

Solving this equation for  $\frac{v_y}{v_x}$  and inserting it into (5.38) yields

$$\begin{aligned} \ddot{\psi} = & -\frac{L^2 C_f C_r}{J_z v_x \sigma} \dot{\psi} - \frac{m \rho}{J_z \sigma} a_y + \frac{L C_f C_r}{J_z \sigma} \delta + \frac{1}{J_z} \left( e + \frac{\rho}{\sigma} \right) S_w + \\ & + \left( \frac{L C_f C_r (k_{\Delta F_{x,f}} - k_{\Delta F_{x,r}})}{J_z \sigma} + \frac{b_f}{2 J_z} \right) \Delta F_{x,f} - \frac{L}{2 J_z \sigma} (C_r c_f (\delta_{f,0} + k_{w,f}) + \\ & + C_f c_r (\delta_{r,0} + k_{w,r})) w \end{aligned} \quad (5.40)$$

where  $\rho = l_r C_r - l_f C_f$ ,  $\sigma = C_r + C_f$  and  $C_j = F_{z,j} c_j$

Introducing the constant

$$a = -\frac{L^2 C_f C_r}{J_z v_x \sigma} \quad (5.41)$$

and the signals

$$\begin{aligned} u = & -\frac{m \rho}{J_z \sigma} a_y + \frac{L C_f C_r}{J_z \sigma} \delta + \left( \frac{L C_f C_r (k_{\Delta F_{x,f}} - k_{\Delta F_{x,r}})}{J_z \sigma} + \frac{s_f}{2 J_z} \right) \Delta F_{x,f} \\ & - \frac{L}{2 J_z \sigma} (C_r c_f (\delta_{f,0} + k_{w,f}) + C_f c_r (\delta_{r,0} + k_{w,r})) w \end{aligned} \quad (5.42)$$

$$d = \frac{1}{J_z} \left( e + \frac{\rho}{\sigma} \right) S_w \quad (5.43)$$

Equation 5.40 is rewritten to:

$$\ddot{\psi} = a \dot{\psi} + u + d \quad (5.44)$$

In order to implement a disturbance observer in a vehicle it needs to be described in discrete form. This is done by converting the system with the zero-order-hold method [5] yielding:

$$\dot{\psi}(k+1) = e^{ah} \dot{\psi}(k) + \int_0^h e^{as} ds (u + d) = e^{ah} \dot{\psi}(k) + \frac{e^{ah} - 1}{a} (u(k) + d(k)) \quad (5.45)$$

An observer without the disturbance is then derived using Equation 5.45.

$$\hat{\dot{\psi}}(k+1) = e^{ah} \hat{\dot{\psi}}(k) + \frac{e^{ah} - 1}{a} u + K(\dot{\psi}(k) - \hat{\dot{\psi}}(k)) \quad (5.46)$$

The estimation error  $\tilde{\dot{\psi}}(k) = \dot{\psi}(k) - \hat{\dot{\psi}}(k)$  which has the following dynamics:

$$\tilde{\psi}(k+1) = (e^{ah} - K)\tilde{\psi}(k) + \frac{e^{ah} - 1}{a}d(k) \quad (5.47)$$

This is then solved for  $d(k)$  yielding

$$d(k) = \frac{a}{e^{ah} - 1}\tilde{\psi}(k+1) - (e^{ah} - K)\tilde{\psi}(k) \quad (5.48)$$

Equation 5.48 needs to be translated one time step backwards since  $\tilde{\psi}(k+1)$  is unknown. An estimate of the side wind disturbance in the previous time step can now be calculated using (5.48) together with (5.43)

$$\hat{S}_w(k-1) = \frac{J_z}{(e + \frac{\rho}{\sigma})} \left( \frac{a}{e^{ah} - 1}\tilde{\psi}(k) - (e^{ah} - K)\tilde{\psi}(k-1) \right) \quad (5.49)$$

$S_w(k-1)$  can be treated as  $S_w(k)$  when the observer has reached steady state or when using a sufficiently small sample time.

### Performance and Robustness

The discrete transfer function between the actual side wind and the estimation error can be determined using Equation 5.46 and 5.49. A state space form with side wind as input and the estimated side wind error as output is presented below:

$$\begin{aligned} \begin{pmatrix} \tilde{\psi}(k+1) \\ \tilde{\psi}(k) \end{pmatrix} &= \begin{pmatrix} e^{ah} - K & 0 \\ 1 & 0 \end{pmatrix} \begin{pmatrix} \tilde{\psi}(k) \\ \tilde{\psi}(k-1) \end{pmatrix} + \begin{pmatrix} b\frac{e^{ah}-1}{a} \\ 0 \end{pmatrix} S_w(k) \\ \tilde{S}_w = S_w - \hat{S}_w &= \begin{pmatrix} -\frac{a}{b(e^{ah}-1)} & \frac{e^{ah}-K}{b} \end{pmatrix} \begin{pmatrix} \tilde{\psi}(k) \\ \tilde{\psi}(k-1) \end{pmatrix} + S_w \end{aligned} \quad (5.50)$$

This state space description yields the following transfer function between  $S_w$  and  $\tilde{S}_w$ .

$$\tilde{S}_w = \frac{\frac{a}{b(1-e^{ah})}z + \frac{e^{ah}-K}{b}}{z(z - e^{ah} + K)} S_w \quad (5.51)$$

This transfer function is asymptotically stable when the poles lie within the unit circle. This criteria is fulfilled when  $|e^{ah} - K| < 1 \Rightarrow -1 + e^{ah} <$

$K < 1 + e^{ah}$  which means that the error of the observed disturbance  $\tilde{S}_w$  will converge to zero under these conditions.

Sensor offsets cause errors in side wind estimation. An expression for the influence of sensor offsets in steady state is obtained by rewriting Equation 5.40 into

$$\Delta \hat{S}_w = \frac{1}{e\sigma + \rho} \left( -\frac{L^2 C_f C_r}{v_x} \Delta \dot{\psi} + \left( LC_f C_r (k_{\Delta F_{x,f}} - k_{\Delta F_{x,r}}) + \frac{b_f \sigma}{2} \right) \Delta(\Delta F_{x,f}) - m\rho \Delta a_y + LC_f C_r \Delta \delta - \frac{L}{2} (C_r c_f (\delta_{f,0} + k_{w,f}) + C_f c_r (\delta_{r,0} + k_{w,r})) \Delta w \right) \quad (5.52)$$

Validation of the side wind estimation was carried out in simulation environment where the estimated side wind was compared to the side wind output from the reference vehicle model CAS-CaDE. As can be seen in Figure 5.7, the estimated value of side wind force is close to the force defined in the simulation environment.

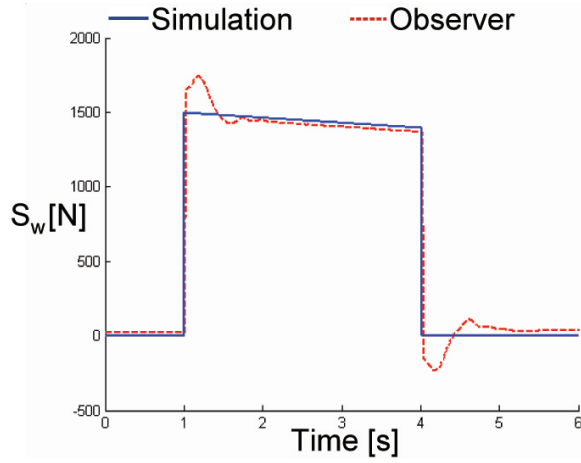


Figure 5.7: Side wind estimation versus side wind output in simulation



## 5.6 Feedforward Control Design

The disturbance estimate can be used to construct controllers that counter act the side wind, see Appendix A. In this section feedforward controllers are designed for three actuators; Active Steering, Brake Steering and Warp Steering. Figure 5.8 shows the control circuit that the design is based on. Consider the one track model in Section 5.4. The general system can be written in state space form together with three control signals and one load disturbance:

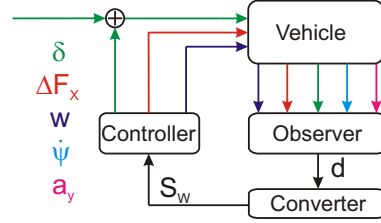


Figure 5.8: Feedforward control with side wind observer

$$\begin{bmatrix} \ddot{\psi} \\ \dot{v}_y \end{bmatrix} = \begin{bmatrix} a_{11} & a_{12} \\ a_{21} & a_{22} \end{bmatrix} \begin{bmatrix} \dot{\psi} \\ v_y \end{bmatrix} + \begin{bmatrix} b_{11} & b_{12} & b_{13} & l_1 \\ b_{21} & b_{22} & b_{23} & l_2 \end{bmatrix} \begin{bmatrix} \delta \\ w \\ \Delta F_{x,f} \\ S_w \end{bmatrix} \quad (5.53)$$

$$y = \dot{\psi}$$

this linear system has the following transfer function

$$\begin{aligned} \dot{\psi} = & \frac{b_{11}(s-a_{22})+b_{21}a_{12}}{(s-a_{11})(s-a_{22})-a_{12}a_{21}}\delta + \frac{b_{12}(s-a_{22})+b_{22}a_{12}}{(s-a_{11})(s-a_{22})-a_{12}a_{21}}w + \\ & + \frac{b_{13}(s-a_{22})+b_{23}a_{12}}{(s-a_{11})(s-a_{22})-a_{12}a_{21}}\Delta F_{x,f} + \frac{l_1(s-a_{22})+l_2a_{12}}{(s-a_{11})(s-a_{22})-a_{12}a_{21}}S_w \end{aligned} \quad (5.54)$$

The idea is to eliminate the disturbance which means that 5.54 shall be equal to zero during the calculation. Assuming that only one control signal will be used at a time, the feedforward transfer functions can be determined for each actuator.

$$\delta = -\frac{l_1(s-a_{22})+l_2a_{12}}{b_{11}(s-a_{22})+b_{21}a_{12}}S_w \quad (5.55)$$

$$w = -\frac{l_1(s-a_{22})+l_2a_{12}}{b_{12}(s-a_{22})+b_{22}a_{12}}S_w \quad (5.56)$$

$$\Delta F_{x,f} = -\frac{l_1(s-a_{22})+l_2a_{12}}{b_{13}(s-a_{22})+b_{23}a_{12}}S_w \quad (5.57)$$

With the model parameters taken from Section 5.4 and 5.5, they may be rewritten into:

$$\delta = -\frac{es + \frac{\sigma + \rho}{mv_x}}{l_f C_f s + \frac{l_f C_f L}{mv_x}} S_w \quad (5.58)$$

$$w = \frac{es + \frac{\sigma + \rho}{mv_x}}{\frac{\xi_1}{2} s + \frac{L(c_f C_r (\delta_{f,0} + k_{w,f}) + c_r C_f (\delta_{r,0} + k_{w,r}))}{2mv_x}} S_w \quad (5.59)$$

$$\Delta F_{x,f} = -\frac{es + \frac{\sigma + \rho}{mv_x}}{\xi_3 s + \frac{C_f C_r L(k_{\Delta F_{x,f}} - k_{\Delta F_{x,r}}) + \frac{b_f}{2} \sigma}{mv_x}} S_w \quad (5.60)$$

The control signals in the feedforward controllers are set points for the vehicle actuators. In order to achieve a good result, the actuators must be fast and accurate i.e. no stationary errors are tolerated since they will be transmitted into the controller if the set points are used as inputs to the observer. When steady state is reached, these controllers will, in the optimal case, eliminate the side wind disturbance completely. Special for the warp and brake controller is that, when driving straight with constant velocity, they are robust against parameter errors in  $k_{\Delta F_{x,f}}$  and  $k_{w,f}$  respectively. Parameter errors will, however, cause a side wind estimate that deviates from the real one that is acting on the vehicle.

## 5.7 Simulation Results

### 5.7.1 Method

The simulations were carried out in Matlab/Simulink. CASCaDE, see section 1.3, acted as the vehicle. The active steering system that was used in this evaluation was modelled with the dynamics between the steering wheel and the wheel. It is assumed that the driver's intended driving path is straight which makes it easier to distinguish the estimated disturbance as side wind since the impact of parameter errors is smaller. The velocity was controlled by a PI controller. In order to measure the impact of side wind and the controllers, the yaw rate  $\dot{\psi}$  was considered together with the longitudinal acceleration  $a_x$  and the control signals for each actuator respectively. These signals gives a good picture of the vehicle behavior. The uncontrolled vehicle is referred to as *REF*, Brake steering is called *BS*, Warp steering *WS* and Active Steering *AS*.

### 5.7.2 Actuator Comparison

The experiments started by evaluating each actuator independently under different circumstances in terms of wind velocity and vehicle velocity. In the first test the wind speed was set to 15 m/s which corresponds to approximately 50 km/h.

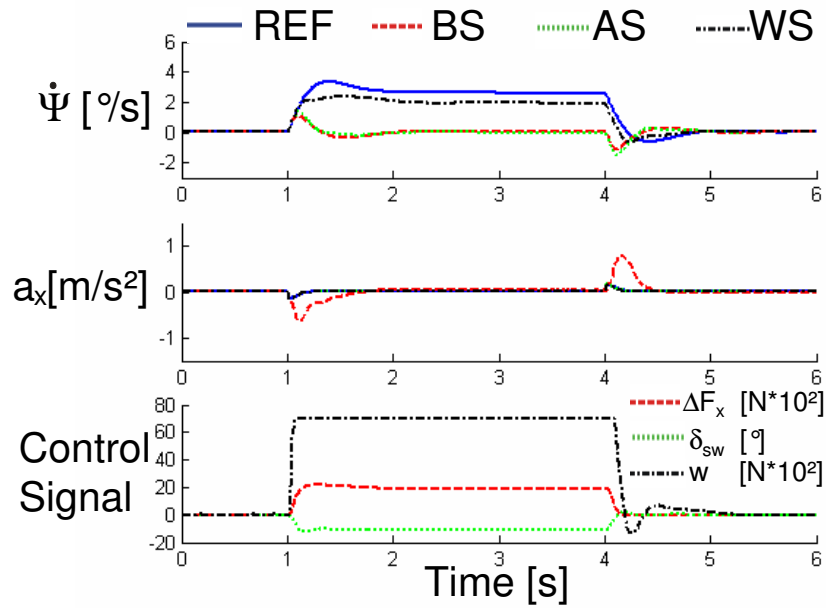


Figure 5.9: Actuator comparison with vehicle velocity 120 km/h and wind velocity 15 m/s

Figure 5.9 clearly shows the effectiveness of active steering control and brake steering control which both eliminated vehicle rotation in less than 0.5 seconds. The warp controller can only reduce the impact slightly since it saturates. Brake steering induces a small negative acceleration which the velocity controller compensates for with a satisfying result.

The second test was carried out under rougher conditions with a wind speed of 25 m/s. When considering  $\dot{\psi}$  in Figure 5.10 both active steering and brake

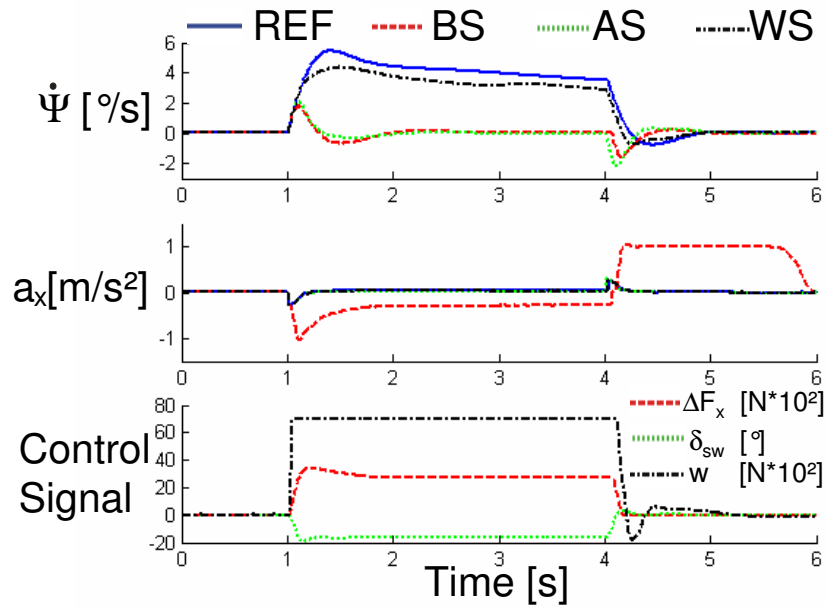


Figure 5.10: Actuator comparison with vehicle velocity 120 km/h and wind velocity 25 m/s

steering eliminated the rotation, but the engine could not provide enough drive torque to compensate the negative longitudinal forces from brake steering. This caused negative acceleration during the side wind influence followed by positive acceleration after the exposure.

The last test was done to investigate the influence of side wind under higher velocities. Therefore the velocity was raised to 160 km/h. When comparing

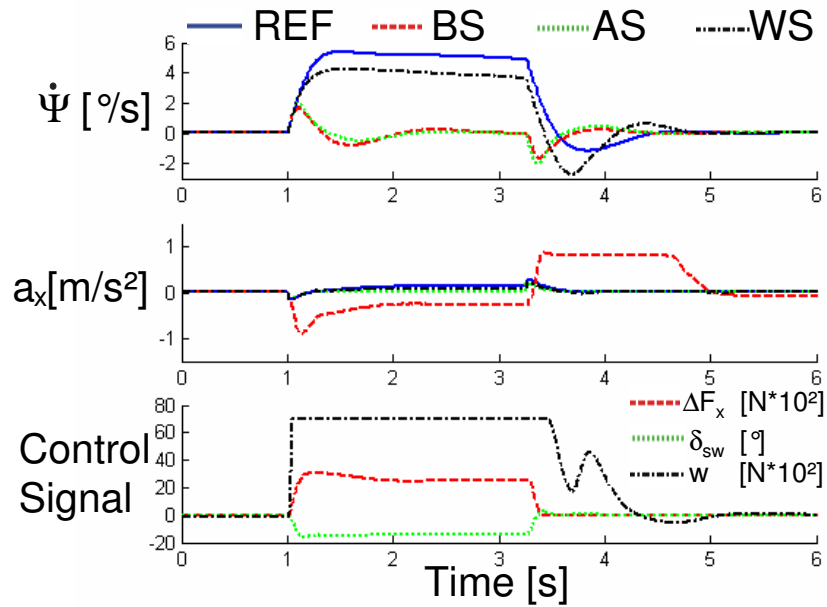


Figure 5.11: Actuator comparison with vehicle velocity 160 km/h and wind velocity 15 m/s

the uncontrolled vehicles behaviour in figure 5.10 and 5.11 it is fairly similar. This also applies for the controlled vehicles behaviour.

### 5.7.3 Simultaneous Actuator Interference

If a vehicle is equipped with more than one of these actuators it is possible to superpose the controllers. The method considered in this report is to use one actuator up to a specified threshold where the second actuator will be activated. When the second actuator output has reached a certain level the third actuator will be switched on. With this method it is possible to customize the coordinated controller with a starting point in comfort, effectiveness etc. depending on where the priority lies. It is also possible to control a large disturbance where each actuator, acting on its own, would be saturated before a satisfying result was achieved.

The order in which the actuators are switched on is as follows:

1. Warp when  $|S_w| > 0$
2. BS when  $|w|$  has reached 6000 N
3. AS when  $|\Delta F_x|$  has reached 1500 N

The disturbance input signal is different for all controllers. The warp controller gets the original disturbance while the brake controller gets the original disturbance minus the part that warp manages to take out. At the end the steering controller gets the part of the disturbance that warp and brake steering have not been able to compensate for.

The results from the simulations are presented below in Figure 5.12 to 5.14. In Figure 5.12 the coordinated controller was used under the same circumstances as the controllers in Figure 5.9.

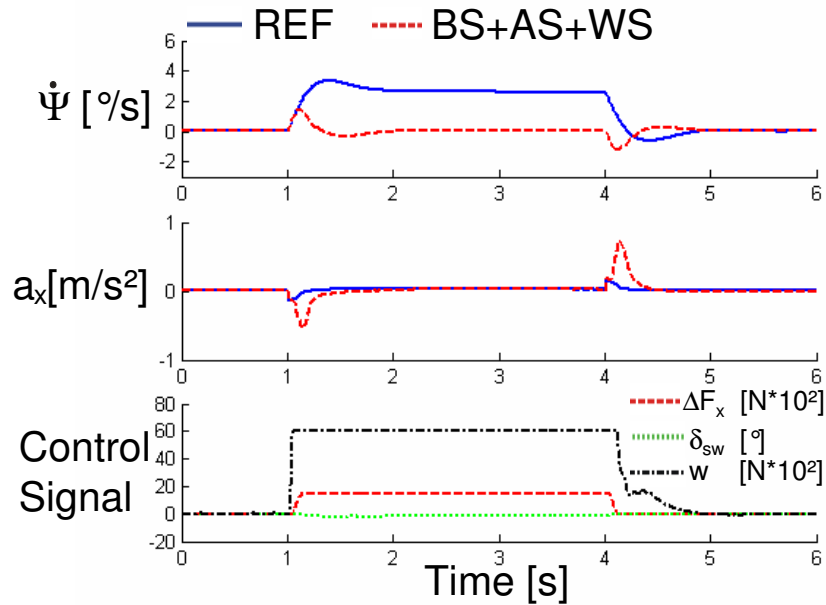


Figure 5.12: Coordinated controller performance with vehicle velocity 120 km/h and wind velocity 15 m/s

The vehicle rotation is eliminated very fast and accurate. When studying the control signals it can be seen that almost no steering action is needed under these circumstances. The initial deceleration is slightly smaller than in the case with brake control. The deceleration can be reduced further by changing the threshold for maximum brake force. This will, however, result in a larger steering intervention.

The second test of the coordinated control strategy was performed with a side wind of 25 m/s, see Figure 5.13.

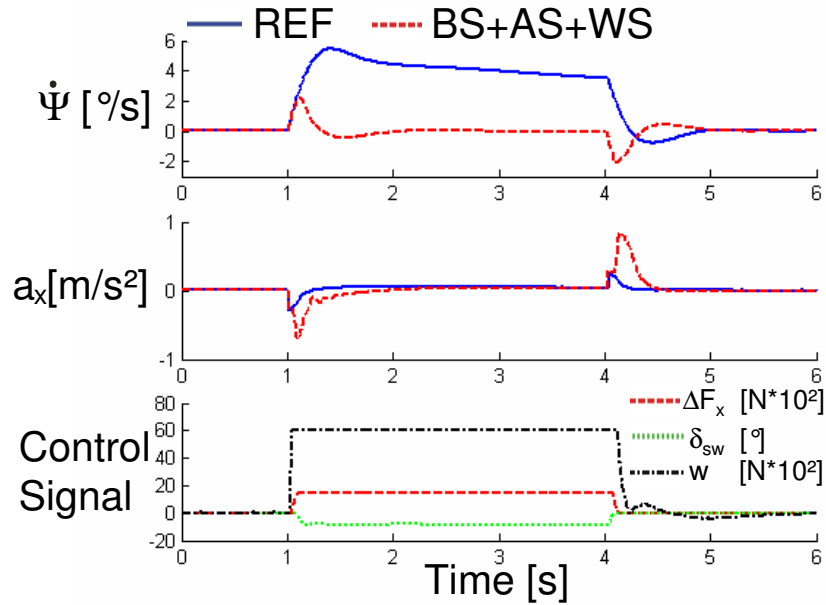


Figure 5.13: Coordinated controller performance with vehicle velocity 120 km/h and wind velocity 25 m/s

Since the magnitude of the maximum brake force was the same in all cases the result in terms of longitudinal acceleration was expected to be equal to the previous experiment. This was not the case, but when studying the uncontrolled vehicle, *REF*, it can be seen that the acceleration has changed there as well compared to the previous setup. This means that there is a dependency between the magnitude of side wind and the longitudinal acceleration.



In the last test the vehicle velocity was increased to 160 km/h. Figure 5.14 shows the results from that simulation.

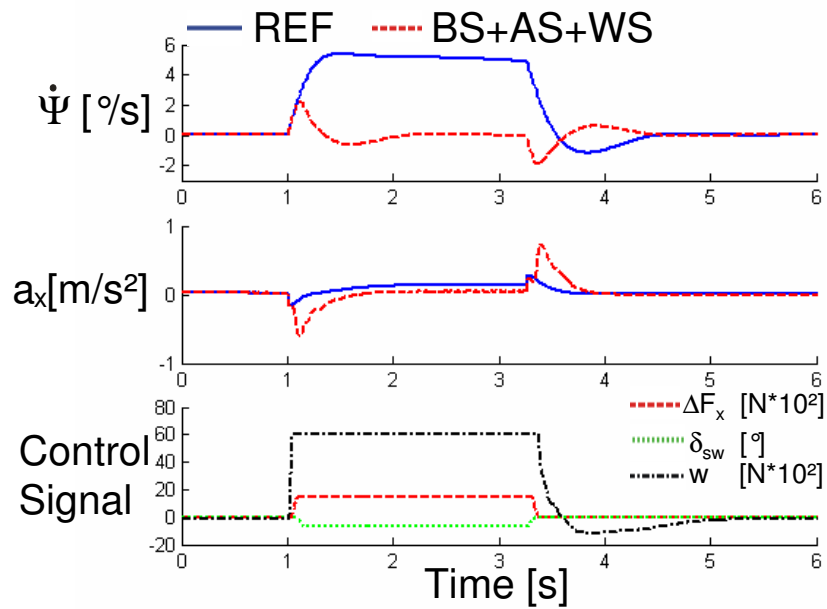


Figure 5.14: Coordinated controller performance with vehicle velocity 160 km/h and wind velocity 15 m/s

As can be seen in the plot, the longitudinal acceleration is smaller than in the previous case.

## 5.8 Results on the Test Track

On one of DaimlerChrysler's test tracks in Stuttgart it is possible to run tests with side wind. Side wind is created by a couple of large fans which together generate a wind velocity of up to 80 km/h. Test results are of great interest when evaluating a control strategy. It is not only measurements that tells if the control strategy is appropriate or not, it is also the driver experience. The control strategy that was implemented in the vehicle was the brake steering system, an approach that was developed in this Master's Project.

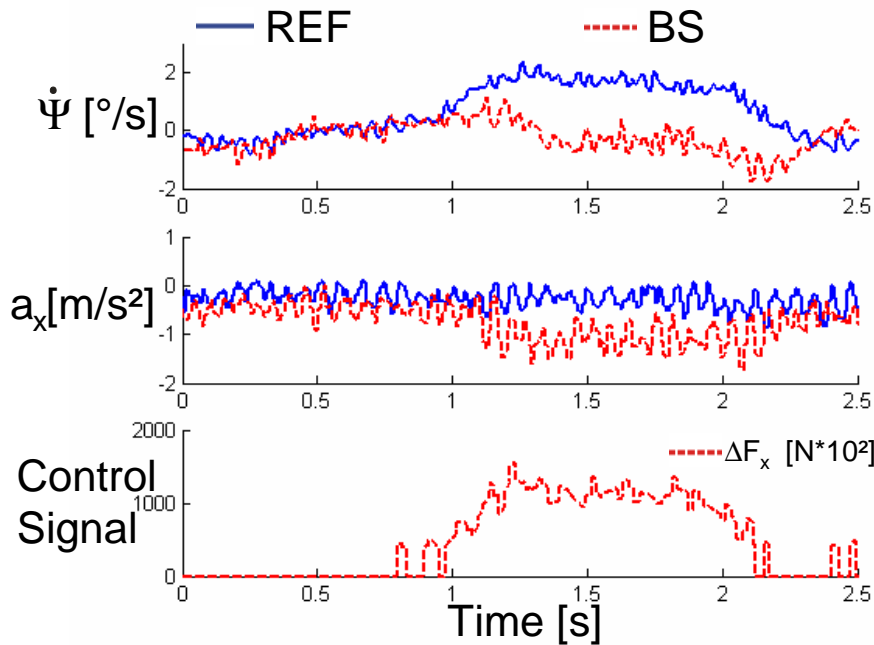


Figure 5.15: Results from test with brake steering control at 120 km/h

When studying Figure 5.15 it can be seen that the controller manages to compensate for the side wind disturbance at a cost of a slight deceleration. This test was carried out without velocity control. If a velocity controller is constructed with a feedforward system that controls the drive torque on the rear axle it is theoretically possible to keep the total longitudinal force at zero during the manoeuvre. It is, however, likely that a small deceleration occurs in the initial phase since it takes longer time to apply drive torque than brake torque with today's systems.

## 5.9 Discussion

The parameters of the model varies with the number of passengers in the vehicle and their position. This is not taken into consideration in the construction of the model. It is affecting the magnitude of the disturbance estimate but, when driving straight, not necessarily the outcome in terms of vehicle rotation. There were several different passenger constellations involved during the test drives and the subjective judgement was that the vehicle behaved predictable and that the control strategy was suitable for the task.

In the simulations an arbitrary steering system was used. The results for active steering on the test track might therefore differ depending on the choice of actuator in the test vehicle, but since today's steering systems are both fast and accurate it will not deviate much. The outcome of suspension steering through warp differs more. The effect is larger in the real vehicle compared to the effect in the vehicle model CASCaDE. This is since some effects are not yet implemented in CASCaDE. The direction in which the vehicle is turning is, however, correct.

The coordinated controller was designed with an approach where suspension steering is used for minor disturbances. The support of brake and/or active steering is added if the disturbance is larger. The result is a comfort oriented strategy with the advantage that only the suspension is used during small disturbances, an active system that already runs at all times due to its other functions. There are, however, other ways of designing a coordinated controller.

Warp steering and active steering were already tested with similar control strategies in other projects, but the results were left out in the test track part of the thesis. This is since the controllers were running in different kinds of vehicles which makes it hard to compare the influence in a fair way.

## 5.10 Conclusions

The controller, consisting of a disturbance observer and a feedforward gain, has been proven suitable for all actuators and under different driving circumstances. It is also ideal for coordinated control since it is possible to distribute the estimated disturbance over several actuators resulting in disturbance elimination.

Regarding the actuators; Both active steering and active brakes have been proven very effective in these simulations. A more extensive evaluation is needed in order to decide which system is the most suitable for production

---

vehicles. The controller uses the ESP sensors to measure  $\dot{\psi}$  and  $a_y$  which indirectly means that the controller will be used in cars equipped with ESP. The advantage of brake steering is then that the hardware already is included in the ESP system which uses dissimilar braking for yaw control. It shall also be kept in mind that an arbitrary steering system was used in the simulations, in the real vehicle will for example the EPS actuator turn the steering wheel which might be uncomfortable or disturbing for some drivers.

# Chapter 6

## $\mu$ – split Braking

### 6.1 Introduction

A typical driving situation during winter is braking with dissimilar friction between the left and the right side of the vehicle. For example these circumstances may occur when braking on a road with bare ground in the middle of the road and snow along the side. This condition is called  $\mu$  – split braking where  $\mu$  – split is defined as the difference between the high- and the low friction coefficient i.e.  $\Delta\mu$ . The result is a disparity in brake forces between the left and the right wheels which creates a yaw torque around the altitude axis making the car turn to the high friction side of the road. Due to the yaw acceleration induced, the driver must interfere and counter steer in order to keep the stability of the vehicle. The situation can quickly become out of control if the driver does not react properly. The current ESP system contains an algorithm that recognizes this situation and reduces the brake pressure on the high friction side giving the driver longer time to react. The increase in stability is on the expense of a longer stopping distance. The conflict between vehicle stability and stopping distance could, however, be solved by interaction of the existing ESP system and other active control systems in the vehicle. This chapter will investigate and discuss how to use the active chassis systems in

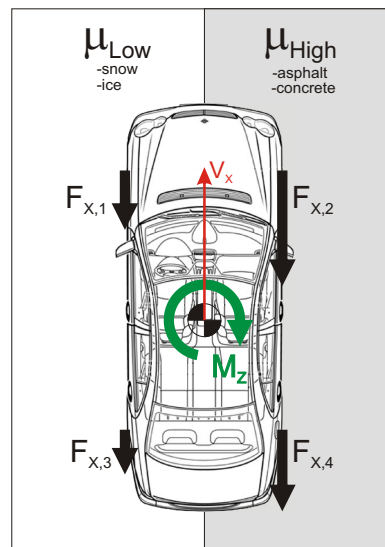


Figure 6.1: Picture of  $\mu$ -split road

order to support the driver during this manoeuvre.

## 6.2 Basics of $\mu$ – split braking

This section presents an approach to explaining how the forces are built up during  $\mu$ -split braking. All calculations are made during steady state and under the assumption of small angles. Consider Figure 6.2. The vehicle is placed in the environment so that the velocity direction is the same as the  $X$ -direction. As a consequence of the steady state approach the acceleration  $a_Y$ , as well as the turning motion  $\ddot{\psi}, \dot{\psi}$  are zero which means that the following applies:

$$\begin{aligned} M_z = & F_{Y,1}(l_f + \frac{b_f}{2}\beta) + F_{Y,2}(l_f - \frac{b_f}{2}\beta) \\ & - F_{Y,3}(l_r - \frac{b_r}{2}\beta) - F_{Y,4}(l_r \cos + \frac{b_r}{2}\beta) \\ & - F_{X,1}(\frac{b_f}{2} - l_f\beta) + F_{X,2}(\frac{b_f}{2} + l_f\beta) \\ & - F_{X,3}(\frac{b_r}{2} + l_r\beta) + F_{X,4}(\frac{b_r}{2} - l_r\beta) = 0 \end{aligned} \quad (6.1)$$

$$\Sigma F_{Y,i} = 0 \quad (6.2)$$

$$\Sigma F_{X,i} < 0 \quad (6.3)$$

In order to describe how the forces are built up during the  $\Delta\mu$  manoeuvre, Chapter 2 needs to be revisited. Expressions for the lateral and longitudinal forces in wheel velocity coordinates, which in this case are parallel to the earth fixed coordinates, are given in Equation 2.15 and 2.16 respectively. The expressions are extended by inserting Equation 2.8, the approximation  $\lambda = \lambda_l$  and (2.13) to become:

$$F_{X,i} = F_{l,i} = \mu_l F_z = \mu \frac{\lambda_l}{\lambda} F_z = (c_1(1 - e^{-c_2\lambda_l}) - c_3\lambda_l) F_{z,i} \quad (6.4)$$

$$F_{Y,i} = F_{s,i} = \mu_s F_z = \mu k_s \frac{\lambda_s}{\lambda} F_z = (c_1(1 - e^{-c_2\lambda_l}) - c_3\lambda_l) k_s \frac{1 + \lambda_l}{\lambda_l} \alpha_i F_{z,i} \quad (6.5)$$

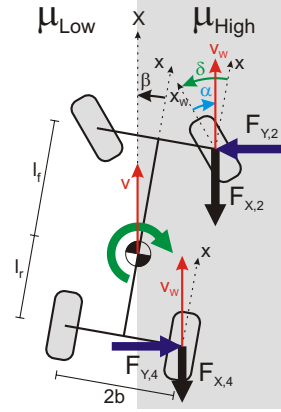


Figure 6.2: Vehicle behavior during  $\mu$  – split braking

The constants in the force descriptions might differ depending on the position of the wheel but that is neglected here. Hence all tire forces are constructed with the same functions.

The ABS system, see Section 3.1 controls the longitudinal wheel slip in the wheel coordinate system. In this project a constant set point  $\lambda_{ref}$  is given to the system. It is assumed that the ABS system reaches its set point and holds it throughout the braking manoeuvre yielding  $\lambda_l = \lambda_{ref} \cos(\alpha) \approx \lambda_{ref} < 0$ . Under these conditions Equation 6.4 and 6.5 can be written as:

$$F_{X,i} = C_{X,i} F_{z,i} \quad (6.6)$$

$$F_{Y,i} = C_{Y,i} \alpha_i F_{z,i} \quad (6.7)$$

where  $C_{Y,i} > 0$  and  $C_{X,i} < 0$ . Note that the constant  $C_Y$  is not the same as  $C_y$  or  $c_y$  which were used in the previous sections under other circumstances. The expressions for  $\alpha_i$  are taken from Equation 2.6 and simplified, under the assumption that  $\beta$  is small and that  $\dot{\psi} = 0$ , to become  $\alpha_1 = \alpha_2 = \delta - \beta$  and  $\alpha_3 = \alpha_4 = -\beta$ . An approximation of  $\beta$  and  $\delta$  in steady state can now be calculated using Equation 6.1 and 6.2. In order to simplify the calculations, forces on the low  $\mu$  side are neglected and in addition are the moment arms chosen such that  $b_f = b_r = b$  and  $l_f = l_r = \frac{L}{2}$ .

$$\begin{aligned} M_z = & C_Y F_{z,2} (\delta - \beta) \left( \frac{L}{2} - \frac{b}{2} \beta \right) \\ & - C_Y F_{z,4} (-\beta) \left( \frac{L}{2} + \frac{b}{2} \beta \right) \\ & + C_X F_{z,2} \left( \frac{b}{2} + \frac{L}{2} \beta \right) \\ & + C_X F_{z,4} \left( \frac{b}{2} - \frac{L}{2} \beta \right) = 0 \end{aligned} \quad (6.8)$$

$$\Sigma F_{Y,i} = C_Y F_{z,2} (\delta - \beta) + C_Y F_{z,4} (-\beta) \quad (6.9)$$

Solving Equation 6.9 for  $\delta$  yields:

$$\delta = \frac{\beta(F_{z,2} + F_{z,4})}{F_{z,2}} \quad (6.10)$$

which inserted in Equation 6.8 gives:

$$M_z = 2C_Y F_{z,4} \beta \frac{L}{2} + C_X F_{z,2} \frac{b}{2} + C_X F_{z,2} \frac{L}{2} \beta + C_X F_{z,4} \frac{b}{2} - C_X F_{z,2} \frac{L}{2} \beta \quad (6.11)$$

By putting  $M_z = 0$  and solving it for  $\beta$  the following expression is achieved:

$$\beta = \frac{-C_X \frac{b}{2} (F_{z,2} + F_{z,4})}{C_Y F_{z,4} L + C_X \frac{L}{2} (F_{z,2} - F_{z,4})} \quad (6.12)$$

This expression is then inserted into (6.10) which yields the required steering angle:

$$\delta = \frac{-C_X b (F_{z,2} + F_{z,4})^2}{F_{z,2} L (C_Y F_{z,4} + C_X \frac{1}{2} (F_{z,2} - F_{z,4}))} \quad (6.13)$$

Since the parameters  $C_Y$  and  $C_X$  are unknown, a heuristic approach is used to determine the sign of the denominator. Once again consider Figure 6.2. In order to achieve force equilibrium during the manoeuvre, a negative force needs to act on the rear wheel. Since  $C_Y$  and  $F_z$  are positive,  $\alpha = -\beta$  must be negative, see Equation 6.7. This in turn means that  $\beta$  is positive which leads to the conclusion that the denominator of Equation 6.12 is positive since the numerator is positive ( $C_X < 0$ ). The same applies for the denominator in Equation 6.13 since it is the same except for a positive scaling factor  $F_{z,2}$ . This knowledge is used in the next section when explaining the effect of the active suspension.

The expressions for  $\beta$  and  $\delta$  were calculated under a number of simplifications but they give a hint of how the vehicle behaviour depends on wheel load and tire characteristics etc.



## 6.3 Applicable Actuators to Support the Driver

### Active Brakes

Modern cars often use an extended ABS system which in addition to the control loop described in Section 3.1 has a feature which helps the driver to control the vehicle during a  $\Delta\mu$  manoeuvre. The system contains two additional parts where the first one is called GMA. Its primary function is to give the driver time to react and counter steer the yaw movement induced by the brake force difference. The second part prevents the stationary brake torque difference from becoming too large, this system is called Select-Low.

The GMA and Select-Low are activated when the estimated friction coefficients differs from each other. The GMA works as a rate limiter for the driver's intended brake torque on the high  $\mu$  side of the vehicle which means that the yaw torque gradually increases until it has reached its final value. The final value is changed by the Select-Low which decreases the set-point value of the slip yielding a smaller brake torque and higher side forces from steering. The gain in steering control results, however, in a longer stopping distance, since the vehicle is not braking at its maximum and it is therefore interesting to find alternative ways to control the vehicle steer ability.

### Active Steering

An active steering system, see Section 3.2 can be used to apply a fast and accurate steering angle as a reaction to the yaw torque induced by the brake forces. With the support from *AS* it is theoretically possible to compensate the impact of the brake torque difference which means that higher brake forces can be used resulting in a shorter stopping distance.

### Active Suspension

It is also of interest to study if the suspension can be used to affect the vehicle behaviour during  $\Delta\mu$ -braking. The impact on the behavior through the force translation needs to be investigated. Consider once again Equation 6.12 and 6.13. In order to show the effect, the wheel loads are extended with a warp term. As can be seen in Section 3.3 the wheel load difference is distributed equally over the wheels.

$$F_{z,1,w} = F_{z,1} + \frac{w}{4} \quad F_{z,2,w} = F_{z,2} - \frac{w}{4} \quad F_{z,3,w} = F_{z,3} - \frac{w}{4} \quad F_{z,4,w} = F_{z,4} + \frac{w}{4} \quad (6.14)$$

The new equations for  $\beta$  and  $\delta$  becomes:

$$\beta = \frac{-C_X b(F_{z,2} + F_{z,4})}{C_Y F_{z,4} L + C_X (F_{z,2} l_f - F_{z,4} l_r) + \frac{w}{4} (C_Y - C_X) L} \quad (6.15)$$

and

$$\delta = \frac{-C_X b(F_{z,2} + F_{z,4})^2}{F_{z,2} (C_Y F_{z,4} L + C_X (F_{z,2} l_f - F_{z,4} l_r)) + \frac{w^2}{16} (C_X - C_Y) L - \frac{w}{4} (2F_{z,2} l_f + (F_{z,2} - F_{z,4}) l_r)} \quad (6.16)$$

It was previously shown that the denominator of  $\beta$  is positive when  $w = 0$ . Since  $(C_Y - C_X)L > 0$  it is easy to see that  $\beta$  will decrease for an increase in  $w$ . The limit of the applied warp depends on both the construction of the suspension system, which can be saturated, as well as on the physical limit  $|\frac{w}{4}| \leq \min(F_{z,i})$ .

The expression for  $\delta$  when  $w = 0$  also has a positive denominator which means that in order to minimize  $\delta$  the maximum of the function  $\frac{w^2}{16} (C_X - C_Y)L - \frac{w}{4} (2F_{z,2} l_f + (F_{z,2} - F_{z,4}) l_r)$  needs to be calculated. By putting the derivative with respect to  $w$  equal to zero and solving it for  $w$ , Equation 6.17 is obtained.

$$w = \frac{-C_X (2F_{z,2} l_f + (F_{z,2} - F_{z,4}) l_r)}{2L(C_Y - C_X)} \quad (6.17)$$

Which yields a maximum since  $\frac{w^2}{16} (C_X - C_Y)L - \frac{w}{4} (2F_{z,2} l_f + (F_{z,2} - F_{z,4}) l_r)$  is convex. The sign of the applied warp that maximizes the function is positive since  $C_Y > 0$  and  $C_X < 0$ . The size given in  $N$  is however not determined since the sizes of  $C_X$  and  $C_Y$  are unknown.

## 6.4 Disturbance Observer for $\mu$ – split braking

There are several approaches to control the steering angle during  $\Delta\mu$ -braking. In this project focus is once again on the disturbance observer with feed-forward control, a control strategy which already has proven its efficiency under side wind disturbances.

In this case the one track model will not be tuned to match the vehicle behaviour under full brake and with differences in adhesion between the tires, since this is not a desired behaviour of the vehicle. The model will instead be tuned under normal driving conditions to act as a reference, hence the

detected disturbance is a function of parameter errors, and also of the brake torque difference  $\Delta F_x$ .

This section describes how to make a steering controller for an arbitrary disturbance. Under the assumption that all disturbances are included in  $d$  and that the effect of warp steering can be neglected, Equation 5.40 can be rewritten as:

$$\ddot{\psi} = -\frac{L^2 C_f C_r}{J_z v_x \sigma} \dot{\psi} - \frac{m\rho}{J_z \sigma} a_y + \frac{L C_f C_r}{J_z \sigma} \delta + d \quad (6.18)$$

This expression is derived with tire side stiffness parameters  $C_f$  and  $C_r$  adapted under non-critical driving conditions. The correction terms needed under braking is included, together with the impact of  $\Delta F_x$ , in  $d$ . This means that the model will not react on the control signals as the actual vehicle when braking but it will maintain steerability during the manoeuvre.

The system is then sampled with the zero-order-hold method

$$\dot{\psi}(k+1) = e^{ah} \dot{\psi}(k) + \int_0^h e^{as} ds (u + d) = e^{ah} \dot{\psi}(k) + \frac{e^{ah} - 1}{a} (u(k) + d(k)) \quad (6.19)$$

where

$$a = -\frac{L^2 C_f C_r}{J_z v_x \sigma} \quad (6.20)$$

and

$$u(k) = -\frac{m\rho}{J_z \sigma} a_y(k) + \frac{L C_f C_r}{J_z \sigma} \delta(k) \quad (6.21)$$

An observer is then derived using Equation 6.19. The error  $d(k)$  is left out which yields:

$$\hat{\dot{\psi}}(k+1) = e^{ah} \hat{\dot{\psi}}(k) + \frac{e^{ah} - 1}{a} u + K(\dot{\psi}(k) - \hat{\dot{\psi}}(k)) \quad (6.22)$$

The observer dynamics are described below in Equation 6.23.

$$\tilde{\dot{\psi}}(k+1) = (e^{ah} - K) \tilde{\dot{\psi}}(k) + \frac{e^{ah} - 1}{a} d(k) \quad (6.23)$$

Solving the equation for  $d(k)$  gives the expression

$$d(k) = \frac{a}{e^{ah} - 1} (\tilde{\psi}(k+1) - (e^{ah} - K)\tilde{\psi}(k)) \quad (6.24)$$

which needs to be translated one time step backwards since there is no information on  $\tilde{\psi}(k+1)$ .

The feedforward gain is calculated with the same method as in the previous application. As in Section 5.6 the control signal will compensate the disturbance completely in the optimal case. Note that active steering is the only system that is controlled by feedforward in this case while the brakes are controlled by the ABS system and warp is independently controlled.

## 6.5 Simulation Results

### 6.5.1 Method

The evaluation was carried out in Simulation using the CASCaDE environment, see Section 1.3. GMA was applied with a rate limiter at the ABS brake torque set point belonging to the high  $\mu$  side of the vehicle. The result is a slower build-up of brake pressure which decreases yaw acceleration in the beginning of the manoeuvre. The implementation of Select-Low was carried out as a scaling of the slip set point  $\lambda_{i,ref}$ . In order to keep the vehicle heading straight, the steering controller has been used in all simulations. GMA and Select Low were tuned until the active steering interference matched the counter steering action of a driver i.e. moderate steering angles and time to apply the steering angle. The ABS slip set point was tuned during braking on dry ground. The stopping distance from  $100km/h$  was 36.7 meters which is considered a good result. When warp is applied, the maximum value is used in order to affect the vehicle side slip angle  $\beta$  as much as possible.

### 6.5.2 Comparison on Snow-Asphalt

The first situation simulated was when braking on a road with snow on one side and asphalt on the other which corresponds to  $\Delta\mu = 0.6$ . The system is oscillating for small velocities which can be seen in all signals in Figure 6.3 to 6.6.  $\beta$  becomes very large when  $v_x$  is close to zero.

### GMA and Select Low

Figure 6.3 shows the most important signals of vehicle stability. It can be seen that, in accordance with the theory, the vehicle side slip angle  $\beta$  was built up, which is necessary in order to create side forces on the rear wheels. The yaw rate had a small peak and was then stabilized around zero within two seconds. The magnitude and slope of the steering action were moderate and the situation can probably be mastered by a driver with average driving skills.

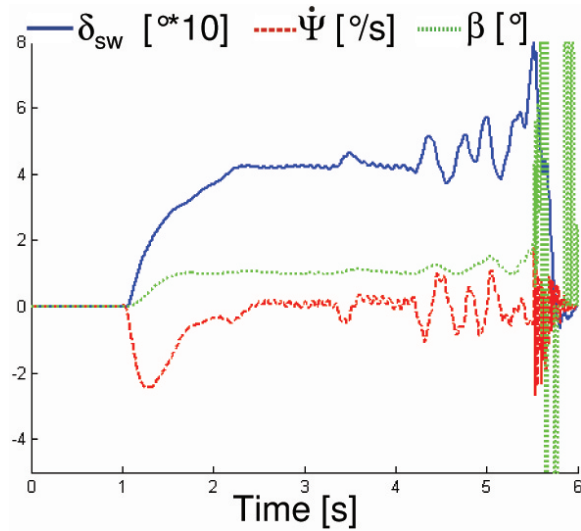


Figure 6.3: GMA+SL

### Active Steering

The result from simulations without GMA/Select Low are shown in Figure 6.4. Initially there was a big peak in yaw rate but the active steering managed to avoid the vehicle from spinning and kept the yaw rate within  $\pm 3$  degrees throughout the manoeuvre. The steering angle needed was about 90 degrees and  $\beta$  was around 3 degrees.

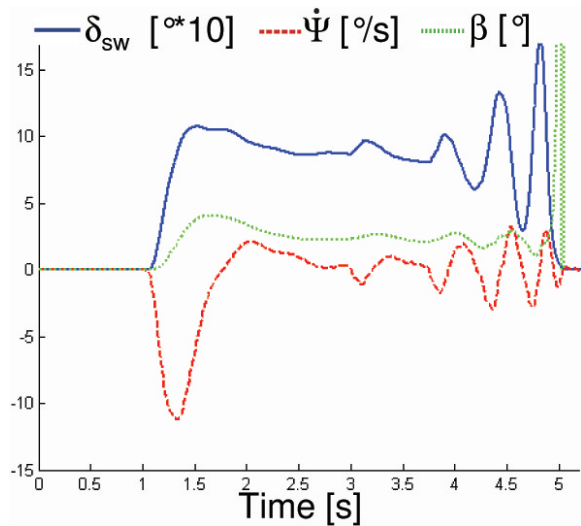


Figure 6.4: AS

### Active Steering and Positive Warp

Consider Figure 6.5. The reason to apply warp under  $\Delta\mu$ -braking was to reduce the side slip and steering angle. A slight change can be seen where  $\beta$  has decreased by approximately 1 degree and the steering angle by 10 degrees. In addition to this, the yaw rate was kept closer to zero. Together these results show a safer and more comfortable braking compared to the previous case.

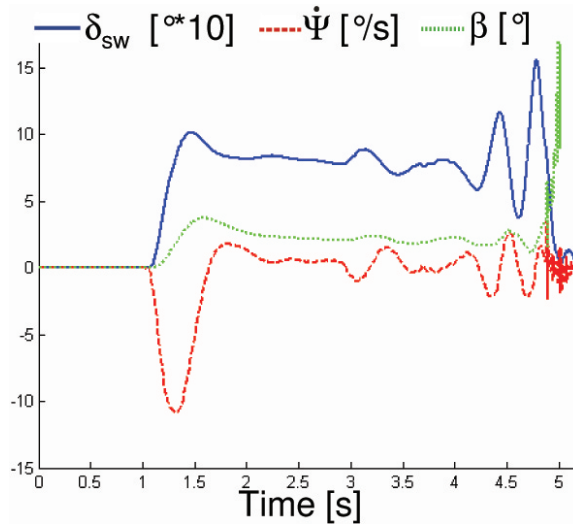


Figure 6.5: AS+PW

### Active Steering and Negative Warp

Negative warp was applied to investigate if the effect on  $\beta$  and steering angle was the opposite compared to the previous case. The signals in Figure 6.6 shows that both the side slip and the steering angle have increased. The behaviour of the vehicle in terms of yaw rate is very much like that in the case without warp.

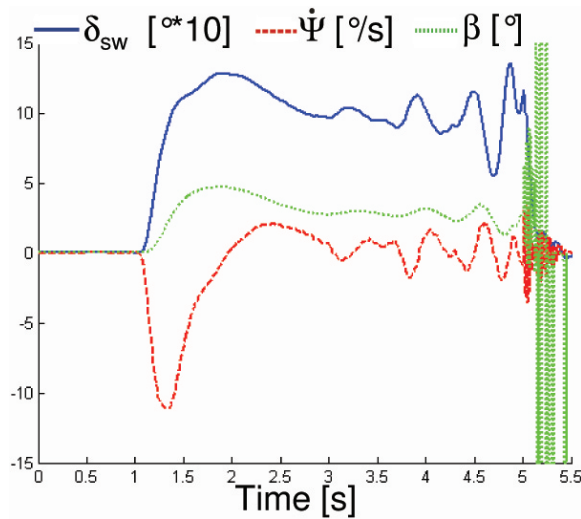


Figure 6.6: AS+NW

### Comparison in Brake Performance

The difference in brake performance is displayed in Figure 6.7. It is clear that reducing the total brake force as in the GMA/SL case has an impact on the stopping distance. This means that under current road conditions a difference of about 10 meters compared to the AS cases. When looking at the setups with AS there is a noticeable increase in stopping distance when using negative warp. AS and AS+PW have almost the same stopping distance with a small advantage for the case with positive warp.

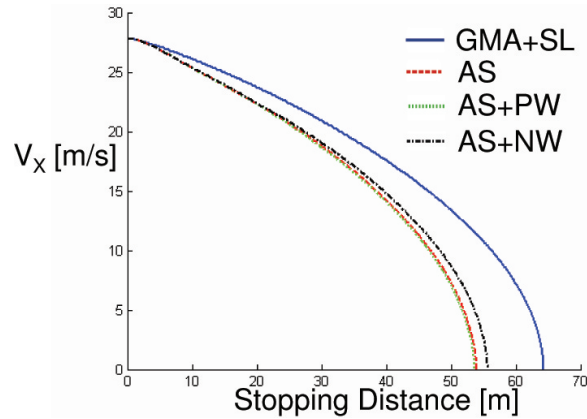


Figure 6.7: Stopping Distance on  $\mu$ -split = 0.6

### Lane Keeping Performance

The results are almost identical regarding the lateral deviation in the simulations. The lateral translation is within 0.25 meters which must be considered a good result under these conditions.

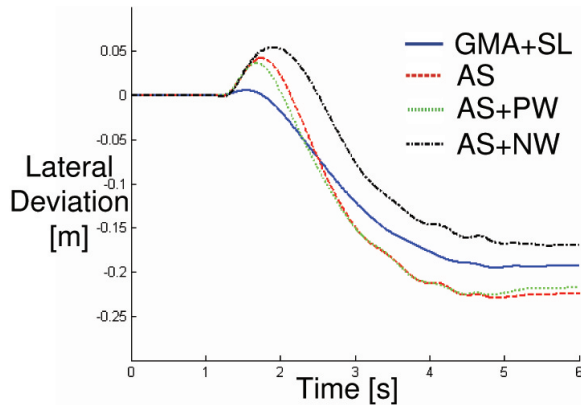


Figure 6.8: Lateral deviation on  $\mu$ -split = 0.6

### Longitudinal and Vertical Forces

The forces that are shown in Figure 6.9 are mean values from the simulations.

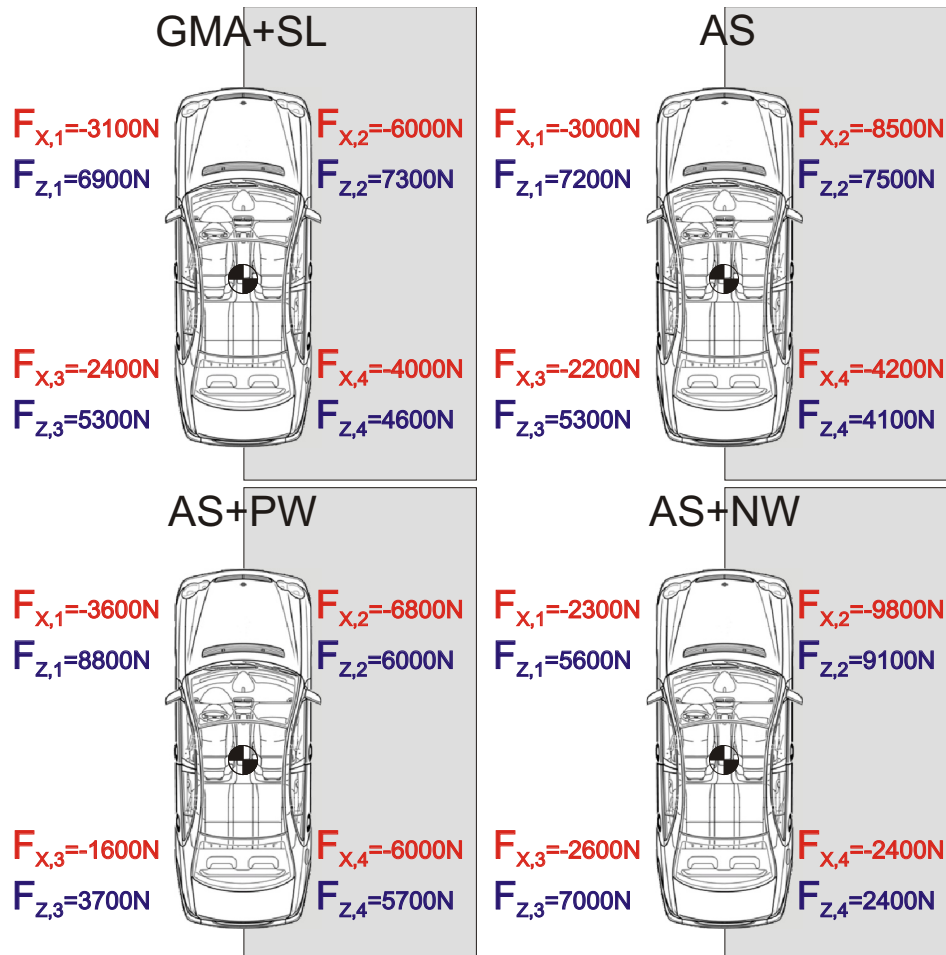


Figure 6.9: Steady state forces for Snow-Asphalt braking

In accordance with the result in stopping distances the total brake forces are approximately the same when comparing AS and AS+PW.

#### 6.5.3 Comparison on Ice-Asphalt

The second situation simulated was when braking on a road with ice on one side and asphalt on the other which corresponds to  $\Delta\mu = 0.9$ .



### GMA and Select Low

Figure 6.10 shows the result from the GMA+SL strategy. The sizes of the signals are similar to those in the corresponding snow-asphalt simulation. There is however a difference regarding the stability of the signals and that might depend on the small tire slip set points on the high  $\mu$  side of the vehicle. The small reference values are easier to control for the ABS system since they are far away from the nonlinear region.

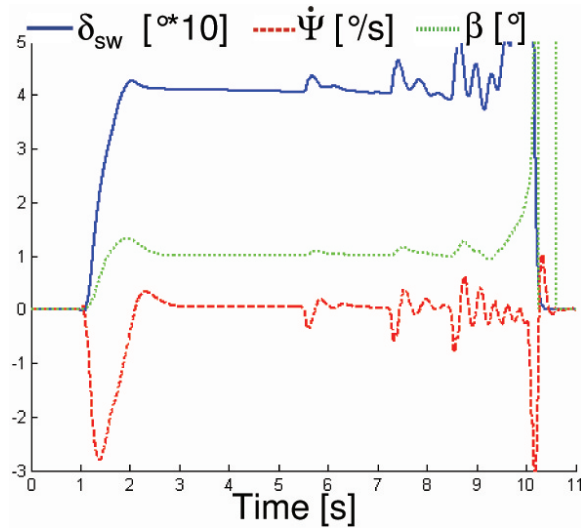


Figure 6.10: GMA+SL

### Active Steering

When GMA and SL were deactivated the following result was achieved, see Figure 6.11. The initial peak of the yaw-rate was very large but the active steering system managed to counter steer and control the turning motion. This required, however, a fast interference and a large steering angle which might be hard to achieve with some steering systems. The steering angle and vehicle side slip angle stabilizes around  $175^{\circ}$  and  $6^{\circ}$  respectively.

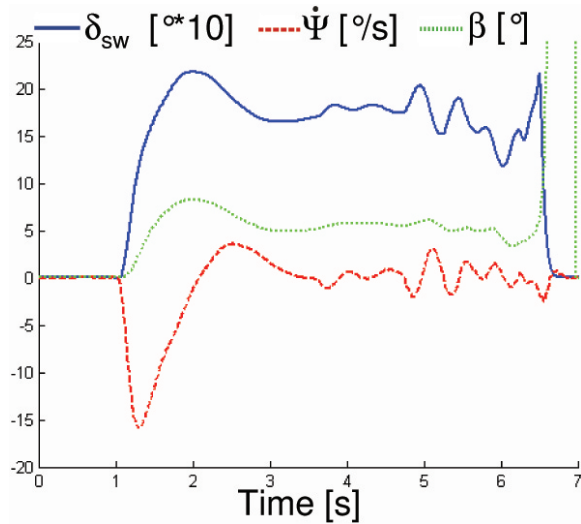


Figure 6.11: AS

### Active Steering and Positive Warp

Figure 6.12 shows the results in the setup with active steering and positive warp. When comparing the signals in this simulation with the previous a major difference is observed regarding both  $\beta$  and  $\delta$ . The side slip has decreased by approximately  $2^\circ$  and  $\delta$  by  $20^\circ$ . The initial peak in steering angle is even smaller which is good for the steering system and the safety in general.

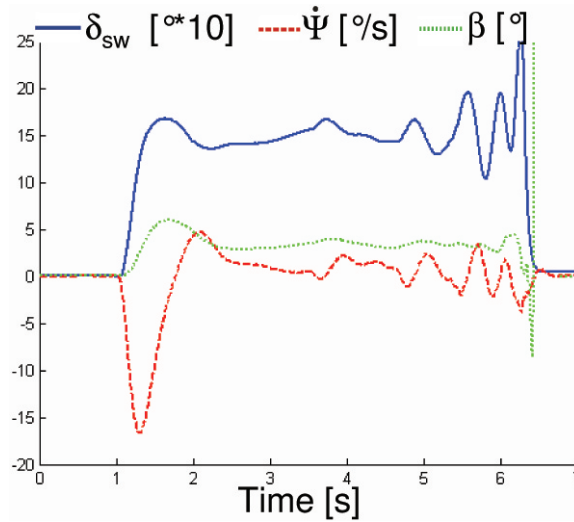


Figure 6.12: AS+PW

### Active Steering and Negative Warp

Figure 6.13 shows the results in the setup with active steering and negative warp. The wheel load on the rear axle is here translated to the low  $\mu$  wheel. According to Equation 6.15 this yields an increase in  $\beta$  in order to reach steady state. The result under these extreme circumstances was a turning motion that was not compensated by the side forces before all wheels were on the low  $\mu$  surface. With all wheels on the ice, steady state was reached but the deceleration and the effect from steering was very poor due to the lack of traction. It will therefore not be considered in the discussion of brake performance below.

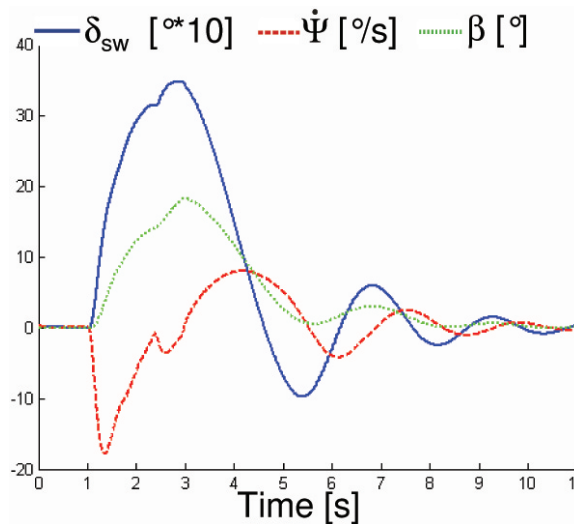


Figure 6.13: AS+NW

### Comparison in Brake Performance

When comparing the control strategies from a brake performance point of view it is clear that under these extreme conditions a system configured without active steering will be at a disadvantage. In order to give the driver support to control the braking a vast interference from the active brake systems was needed. This reflects in the stopping distance which is about 60 meters longer in the GMA/Select Low case.

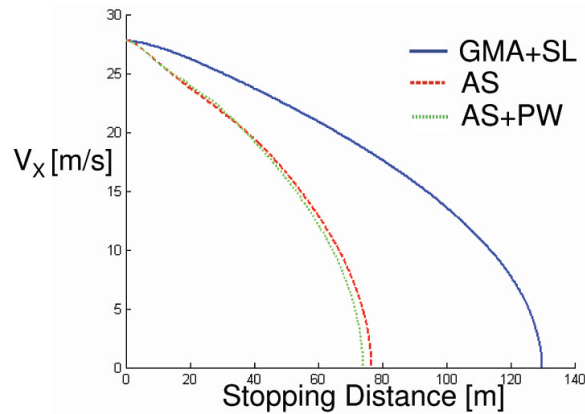


Figure 6.14: Stopping Distance on  $\mu$ -split = 0.9

There is also a difference between AS and AS+Warp. The warp setup does not only have a stabilizing effect on the vehicle, it has in addition a significant influence on the braking distance.

### Lane Keeping Performance

The lateral deviation is shown in Figure 6.15. The vehicle stays within 0.5 meters in all simulations. In the AS+PW case an additional steering wheel angle of  $4^\circ$  was added in order to keep it on the track.

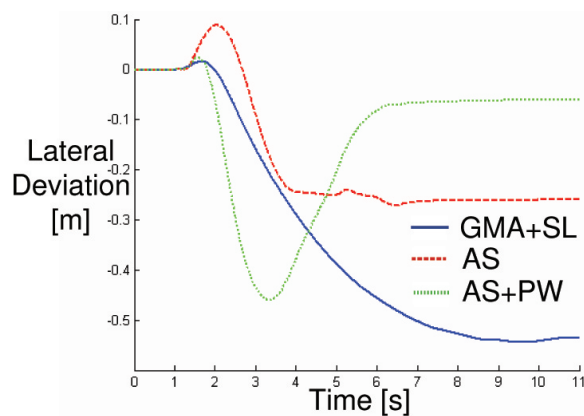


Figure 6.15: Lateral deviation on  $\mu$ -split = 0.9

### Longitudinal and Vertical Forces

The forces in the case with negative warp are not shown in Figure 6.16 since the vehicle left the test track.

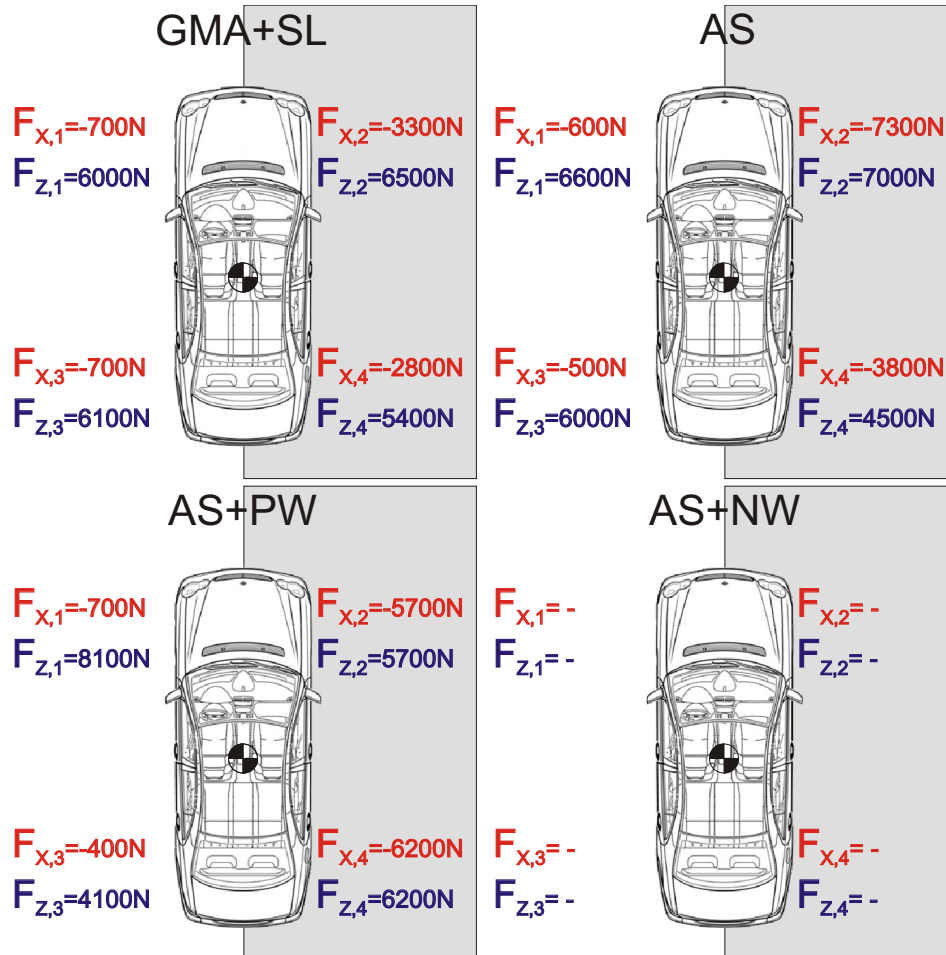


Figure 6.16: Steady state forces for Ice-Asphalt braking

### 6.6 Discussion

The set point of the tire slip values are set to a constant value. When comparing the set point with the simulation output it has been concluded that the ABS system manages to control tire slip in all experiments, but since the results are from simulations this is not necessarily the case in the real vehicle where other effects might occur due to model errors. For example,

changes in wheel load might have additional influences on both the ABS system's control performance as well as steering angle changes. This needs to be investigated further.

In the setup with AS+PW on Ice-Asphalt an additional steering wheel input of  $4^\circ$  was added. This was needed due to the controller that managed to eliminate the rotation with a smaller overshoot than in the other cases. This means that the vehicle is heading in a direction corresponding to  $\int \dot{\psi} = \psi < 0$  which was corrected by driver intervention. An alternative strategy to avoid this problem would have been to control the yaw angle instead of the yaw rate but that signal is not directly measured in the vehicle.

The results from the experiments are consistent. It has been seen that the magnitude of the counter steering angle increases when  $\Delta\mu$  increases. Furthermore, the effect of warp is larger for higher friction differences. Positive warp yields an increase in stability while negative warp gives the opposite result.

The gain in stopping distance when using positive warp can not be seen in the tire force model used for calculations. In order to investigate the effect another model needs to be considered.

Since the magnitude of the stabilizing steering wheel angle can be very large, a steering actuator that does not turn the steering wheel is preferable. When using such a system the driver does not have to change the steering wheel grip. This makes it easier for the driver to apply additional steering angles for lane keeping etc.

## 6.7 Conclusions

The results show a clear gain in brake performance achieved by an active steering system that can compensate for a high brake force difference, they also show the stabilizing effects of positive warp which is in accordance with the hypothesis. What was not expected is the effect that AS+PW has on the stopping distance. With an advantage of almost 3 meters compared to AS on  $\Delta\mu = 0.9$  it implies that warp can be used for stabilization and stopping distance reduction simultaneously. This needs, however, to be investigated further.

The steering control system, a disturbance observer and a feedforward gain, has been proven applicable also for this manoeuvre. Its simplicity and versatility together with its accuracy and rapidness makes it a very good concept for vehicle dynamics control.

## Chapter 7

# Global Control Concept

This chapter presents a concept for global control of the vehicle. Focus is on making an architecture that includes the previously derived controllers in Chapter 5 and 6, but the idea is that it shall be possible to extend the concept by introducing new controllers for other circumstances. Since there are many ways of creating such a system and that the design of a fully functioning system is out of the scope for this thesis, this section is discussing a solution implicitly.

### 7.1 Concept Design

The architecture of a global control system may consist of subdomains as in the proposal shown in Figure 7.1. It is possible to use the previously derived disturbance observers for both situations. With this approach, the control signals will be distributed over the active systems based on measured signals that is present in the vehicle. This is necessary since the disturbance observers will interpret the actuator interference in different ways. One example is when braking on  $\mu$ -split. The  $\mu$ -split observer will detect a disturbance in brake force while the side wind observer will see it as brake steering which is not considered a disturbance in the side wind control system.

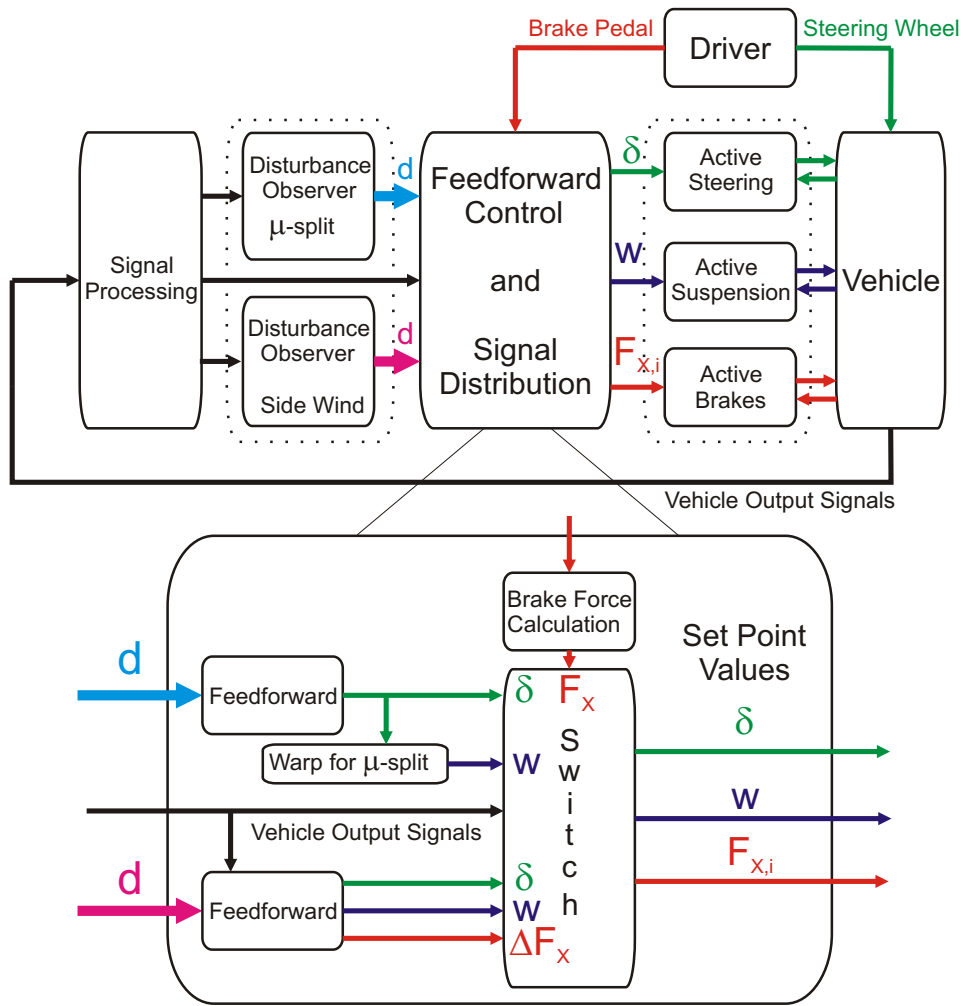


Figure 7.1: Scheme of the control architecture

## 7.2 Criteria

It can be concluded that both systems should not be active simultaneously since they interfere with each other. The first step is therefore to set up criteria for when the controllers shall be activated or deactivated. One starting point is to let the side wind controller run as default and then switch to  $\mu$ -split control when having a certain deceleration or when the driver's desired brake force is above a specific level.

The criteria on when and how the actuators should interfere are, of course, depending on the systems that are present in the vehicle. If the vehicle has an active suspension one idea is to use the coordinated strategy, see Section 5.7, for side wind. This controller will, for small disturbances, only use warp which is part of the active suspension that always runs as opposed to active brakes. If needed, an additional actuator can be switched on when warp saturates. If the vehicle only is equipped with active brakes, the solution would be to set a threshold value for the estimated disturbance to keep the vehicle from braking for the smallest disturbances. This threshold needs to be set so that normal driving does not create signals that cause the brakes to intervene.

When the driver pushes the brake pedal the desired brake force is calculated. If it is higher than a predetermined level, the side wind controller can be taken out of action and be replaced by the  $\mu - split$  system. Depending on whether the vehicle has active steering or not, two starting points need to be considered. With an effective active steering system it is possible to brake without GMA/SL or maybe use a fast GMA that just keeps the initial yaw rate at a moderate level. This yields large improvements in braking performance compared to existing systems on the market. Without active steering, the GMA/SL will be used as in today's production cars and a disturbance observer is then not necessary since there already exists other systems to detect  $\mu - split$ . According to the results in the previous chapter, active suspension shall be used if available. It affects the stability and it might be possible to increase the brake pressure slightly, with maintained controllability, even in the case without active steering.



# Chapter 8

## Outlook

### 8.1 Conclusions

A linear onetrack model was derived with three control signals and one disturbance. The control signals were steering angle, brake force difference between the left and the right side of the vehicle and suspension steering. The effect of brake force difference was investigated and a suitable model of the influence it has on the vehicle behavior was derived. A previously presented onetrack model with steering angle and suspension steering as inputs was considered and successfully extended by including brake steering.

In the side wind situation a disturbance observer based on the extended onetrack model was constructed and used together with feedforward control to eliminate the impact of the disturbance. Brake, suspension and active steering were compared separately in order to evaluate each systems advantages and disadvantages regarding comfort and efficiency. A control strategy where the actuators were superposed to each other was derived in order to show the possibility of integrated control. The brake steering control strategy was then implemented in a test vehicle and benchmarked with satisfying results.

In the  $\mu - split$  situation the disturbance observer was reduced to only include steering angle as input signal. The disturbance in this case consisted of two parts. The first part was the uneven brake forces that appear when braking on a ground with different friction between the left and the right side of the vehicle. The second part was parameter dependent since the onetrack model acts with a reference behavior which means that the parameters are adapted under ideal driving circumstances. In addition to this was the impact of normal force translation investigated analytically and then tested in simulation which gave promising results including increased stability and

a possible decrease in stopping distance.

## 8.2 Future Work

In the side wind case, alternative coordination strategies can be tested and compared to that presented in this project. A profound study of the actuator's own controllers, e.g. the control loop of ABS, needs to be done. This might reveal negative interference such as a shared resonance frequency which causes extensive oscillations under certain conditions.

The  $\mu - split$  controller needs to be evaluated on the test track. It is of interest to develop methods to tune the controller in such a way that GMA and AS together assure a moderate yaw rate in the initial phase of the brake manoeuvre. An extended study of the strategy where warp is added during  $\mu - split$  braking is also an interesting topic. Is the stopping distance a function of warp? Is it possible to find explicit values of warp that minimize the counter steering angles under different circumstances?

Regarding global control; Systems that are constructed for test vehicles with certain actuator constellations need to be designed and evaluated. It is possible to introduce other active systems such as a drive torque distribution system which can be added in future coordination controllers.

# Appendix A

## Control Theory

In the following chapter methods for dynamic system analysis and control are presented.

### A.1 Dynamical System Representation

A general autonomous dynamical system can be represented by a set of differential equations on the form

$$\dot{\mathbf{x}} = \mathbf{f}(\mathbf{x}, t) \tag{A.1}$$

where  $\mathbf{x}$  is an  $n \times 1$  state vector and  $\mathbf{f}$  is an  $n \times 1$  vector function. The solution  $\mathbf{x}(t)$  corresponds to a curve in state space which is called the system trajectory.

A special class of dynamical systems are the linear time invariant systems. They can be described in the following manner which is called state-space form

$$\dot{\mathbf{x}} = \mathbf{A}\mathbf{x} \tag{A.2}$$

where  $\mathbf{A}$  is an  $n \times n$  matrix. The system is stable if the eigenvalues of  $\mathbf{A}$  have a real part that is less than zero. In this case the system will converge to  $\mathbf{x} = \mathbf{0}$  for all initial conditions.

In order to control the system, additional signals need to be added to the representation. Together with an input signal vector  $\mathbf{u}$  and an output signal vector  $\mathbf{y}$  the following state-space form is used:

$$\begin{aligned}\dot{\mathbf{x}} &= \mathbf{A}\mathbf{x} + \mathbf{B}\mathbf{u} \\ \mathbf{y} &= \mathbf{C}\mathbf{x} + \mathbf{D}\mathbf{u}\end{aligned}\tag{A.3}$$

where  $\mathbf{u}$  is an  $m \times 1$  vector,  $\mathbf{B}$  is an  $n \times m$  matrix,  $\mathbf{C}$  is an  $r \times n$  matrix and  $\mathbf{D}$  is an  $r \times m$  matrix. By Laplace transforming the system a representation that describes the dependency between the output and input signal can be derived. This representation is called *transfer function* and it is calculated as follows:

$$\mathbf{y} = (\mathbf{C}(s\mathbf{I} - \mathbf{A})^{-1}\mathbf{B} + \mathbf{D})\mathbf{u}\tag{A.4}$$

## A.2 Feedforward Control

There are several situations where disturbances are acting on the vehicle. These disturbances can be compensated for by different control strategies. In this project focus is on feedforward control. The feedforward control is constructed under assumption that the disturbance is known.

If the transfer function relating the output  $\mathbf{y}$  to the disturbance  $D$  and the control signal  $\mathbf{u}$  are  $G_D$  and  $G_P$ , the transfer function  $G_{FF}$  of the feed forward controller should be

$$G_{FF} = -G_p^{-1}G_D\tag{A.5}$$

which in the optimal case compensates the disturbance completely. The design of the feedforward compensator in this project is calculated as in Equation A.5 and then reduced to a constant gain, see [5], under the assumption of stationary disturbances.

## A.3 Disturbance Observer

In order to construct a feedforward controller the disturbance needs to be known. In some cases disturbance measurements are not available or unreliable. This section presents a strategy to overcome this problem by estimating the disturbance. The idea is taken from [4]

Consider the system described below

$$\begin{aligned}\dot{\mathbf{x}} &= \mathbf{A}\mathbf{x} + \mathbf{B}(u + d) \\ y &= \mathbf{C}\mathbf{x}\end{aligned}\tag{A.6}$$

where  $d$  is the disturbance,  $\mathbf{x} = (x_1 \ x_2)^T$  and

$$A = \begin{pmatrix} a_{11} & a_{12} \\ a_{21} & a_{22} \end{pmatrix} \quad B = \begin{pmatrix} b_1 \\ b_2 \end{pmatrix} \quad c = ( \ 1 \ 0 ) \quad (\text{A.7})$$

With this system a linear observer is derived under the assumption that no disturbance is present.

$$\begin{aligned} \dot{\hat{\mathbf{x}}} &= A\hat{\mathbf{x}} + Bu + K(y - \hat{y}) \\ \hat{y} &= C\hat{\mathbf{x}} \end{aligned} \quad (\text{A.8})$$

The estimation error is then defined as ( $\tilde{\mathbf{x}} = \mathbf{x} - \hat{\mathbf{x}}$ ). By inserting (A.6) and (A.8) into the expression for  $\tilde{\mathbf{x}}$  it yields the following dynamics

$$\dot{\tilde{\mathbf{x}}} = (A - KC)\tilde{\mathbf{x}} + Bd \quad (\text{A.9})$$

where  $K$  is chosen in such way that  $\tilde{\mathbf{x}}$  will converge. When the estimation error has reached steady state ( $\dot{\tilde{\mathbf{x}}} = 0$ ) Equation A.9 is solved for  $d$ . The following expression for the disturbance is achieved.

$$d = -B^{-1}(A - KC)\tilde{\mathbf{x}} \quad (\text{A.10})$$

## A.4 Disturbance Observer with Feedforward Control

The system achieved when connecting a disturbance observer with a feedforward controller has interesting characteristics which are investigated in an example below. The process that is to be controlled is a first order system with one control signal and one disturbance. The system is presented below in Figure A.1

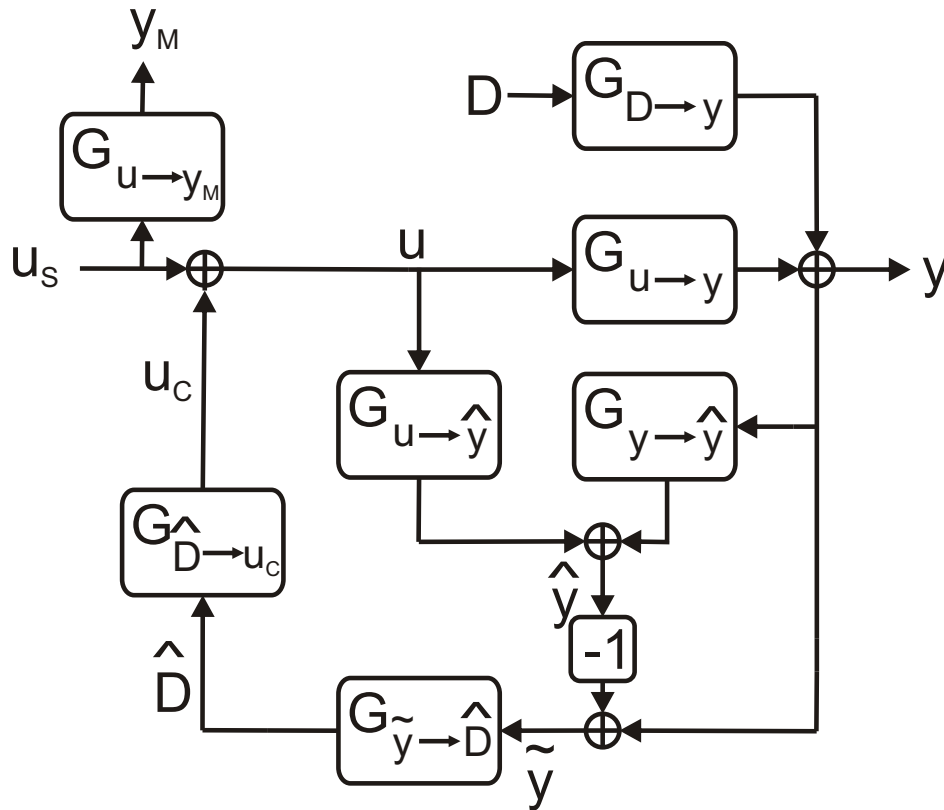


Figure A.1: Control Scheme

### Transfer Functions

The process dynamics are represented by the transfer functions  $G_{u \rightarrow y}$  and  $G_{d \rightarrow y}$  which are calculated below:

$$\begin{aligned} \dot{x} &= ax + bu + b_d d \\ y &= x \end{aligned} \Rightarrow y = \frac{b}{s-a}u + \frac{b_d}{s-a}d \quad (\text{A.11})$$

where the exact value of the parameters  $a$ ,  $b$  and  $b_d$  are unknown.

The signal  $y_M$  represents the output from the modelled process without disturbance. The input  $u_s$  is an external control signal given outside the system. The dynamics of the model are described by  $G_{u \rightarrow y_M}$  which is derived below:

$$\begin{aligned} \dot{x}_M &= \hat{a}x_M + \hat{b}u_s & \Rightarrow & y_M = \frac{\hat{b}}{s - \hat{a}}u_s \\ y_M &= x_M \end{aligned} \quad (\text{A.12})$$

where  $\hat{a}$  and  $\hat{b}$  are model parameters designed to correspond to  $a$  and  $b$ .

The transfer functions  $G_{u \rightarrow \hat{y}}$  and  $G_{y \rightarrow \hat{y}}$  are calculated as follows:

$$\begin{aligned} \dot{\hat{x}} &= (\hat{a} - k)\hat{x} + \hat{b}u + ky & \Rightarrow & \hat{y} = \frac{\hat{b}}{s - \hat{a} + k}u + \frac{k}{s - \hat{a} + k}y \\ \hat{y} &= \hat{x} \end{aligned} \quad (\text{A.13})$$

It can be seen that the dynamics of the observer are based on the model parameters together with a constant  $k$  that is chosen so that it assures observer convergence.

When calculating the observer error  $\tilde{y} = y - \hat{y}$ , Equation A.11 and A.13 are used yielding the dynamics below:

$$\begin{aligned} \dot{\tilde{x}} &= (a - k)\tilde{x} + (b - \hat{b})u + (a - \hat{a})\hat{y} + b_d d & \Rightarrow & \\ \tilde{y} &= \tilde{x} & & \\ & \Rightarrow \tilde{y} = \frac{b - \hat{b}}{s - a + k}u + \frac{a - \hat{a}}{s - a + k}\hat{y} + b_d d \end{aligned} \quad (\text{A.14})$$

Since  $a$ ,  $b$  and  $b_d$  are unknown the estimate of the disturbance will be calculated, using a modelled gain  $\hat{b}_d$  and with the intention that  $a = \hat{a}$  and  $b = \hat{b}$ , as:

$$\hat{d} = \frac{(s - \hat{a} + k)}{\hat{b}_d}\tilde{y} \quad (\text{A.15})$$

This estimate will not only include  $d$  but also parameter errors.

The feedforward controller is designed in accordance with Equation A.5 where the transfer functions are based upon the process model  $y_m = \frac{\hat{b}}{s - \hat{a}}u + \frac{\hat{b}_d}{s - \hat{a}}d$ . This yields the following relationship between  $\hat{d}$  and  $u_c$ :

$$u_c = -\frac{\frac{\hat{b}_d}{s - \hat{a}}\hat{d}}{\frac{\hat{b}}{s - \hat{a}}}\hat{d} = \frac{\hat{b}_d}{\hat{b}}\hat{d} \quad (\text{A.16})$$

#### A.4.1 The Closed Loop

In order to calculate the transfer function the following insertions were made: Equation (A.13)  $\rightarrow$  (A.14)  $\rightarrow$  (A.15)  $\rightarrow$  (A.16)

Together with the relation  $u = u_c + u_s$  the new equation is solved for  $u_c$  yielding:

$$u_c = \frac{\hat{a} - a}{b(s - \hat{a} + k)}y + \frac{\hat{b}(s - a + k) - b(s - \hat{a} + k)}{b(s - \hat{a} + k)}u_s - \frac{b_d}{b}d \quad (\text{A.17})$$

When inserting (A.17) into (A.11) and solving it for  $y$  the following expression is achieved:

$$y = \frac{\hat{b}}{s - \hat{a} + k}u_s = y_m \quad (\text{A.18})$$

This implies that the system compensates the disturbance  $d$  perfectly but the parameter errors stays and the process is forced to behave as the model. This system is however nonrealizable since the transfer function in (A.15) is not proper. This can be solved in two ways. One way is to take the steady state gain and the other way is to add a filter to the expression. The new expressions then becomes  $\hat{d} = \frac{(-\hat{a}+k)}{\hat{b}_d}\tilde{y}$  and  $\hat{d} = G_f \frac{(s-\hat{a}+k)}{\hat{b}_d}\tilde{y}$  respectively. Using the second approach with a filter  $G_f = \frac{\omega_f}{s+\omega_f}$  the expression for  $y$  becomes:

$$y = \frac{\hat{b}\hat{b}(\omega_f + s)}{\hat{b}s^2 + (\omega_f b - \hat{b}a)s - \omega_f \hat{b}a}u_s + \frac{s\hat{b}d}{\hat{b}s^2 + (\omega_f b - \hat{b}a)s - \omega_f \hat{b}a}d \quad (\text{A.19})$$

The system is stable if  $(\hat{b})$ ,  $(\omega_f b - \hat{b}a)$  and  $(-\omega_f \hat{b}a)$  have the same sign. If the process is stable ( $a, \hat{a} < 0$ ) and the filter is stable ( $\omega_f > 0$ ) this means that  $(\text{sign}(b) = \text{sign}(\hat{b}))$ . Furthermore must  $|\omega_f b| > |\hat{b}a|$  in order to fulfil the criteria.

The convergence for a constant input signal ( $u_s = \frac{u_{const}}{s}$ ) and a constant disturbance  $d = \frac{d_{const}}{s}$  is calculated with the final value theorem to become:

$$\lim_{t \rightarrow \infty} y = \lim_{s \rightarrow 0} s y = \frac{\hat{b}}{-\hat{a}} u_{const} = \lim_{t \rightarrow \infty} y_M \quad (\text{A.20})$$

The output signal of the process converges to the output signal of the model. When changing the disturbance input to a ramp  $d = \frac{d_{const}}{s^2}$ , the final value theorem yields the same result.



### Set Point Control

Due to the result that  $y(\infty) = y_M(\infty)$  for a constant input signal it is interesting to investigate if the system can be used as a set point controller. When rewriting (A.12) with  $y_M$  as input signal and  $u_s$  as output signal it yields  $u_s = \frac{s-\hat{a}}{\hat{b}}y_M$  which needs to be filtered in order to be realizable:

$$u_s = \frac{w_{f2}(s - \hat{a})}{\hat{b}(s + \omega_{f2})} y_M \quad (\text{A.21})$$

Inserting (A.21) into (A.19) yields the following transfer function from  $y_M$  to  $y$ :

$$y = \frac{\hat{b}\hat{b}(\omega_f + s)}{\hat{b}s^2 + (\omega_f b - \hat{b}a)s - \omega_f b \hat{a}} \cdot \frac{w_{f2}(s - \hat{a})}{\hat{b}(s + \omega_{f2})} y_M + \frac{s\hat{b}d}{\hat{b}s^2 + (\omega_f b - \hat{b}a)s - \omega_f b \hat{a}} d \quad (\text{A.22})$$

where  $y_M$  is treated as a set point value of  $y$ . The system in (A.22) inherits the poles and zeros from (A.19) but adds an additional zero and pole. The extension of the stability criterion stated above is that  $\omega_{f2} > 0$ .

The output error  $y_e = y_M - y$  is presented below:

$$y_e = \frac{(\hat{b}(s+\omega_{f2}))(\hat{b}s^2+(\omega_f b-\hat{b}a)s-\omega_f b \hat{a})-(\hat{b}\hat{b}(\omega_f+s))(w_{f2}(s-\hat{a}))}{(\hat{b}(s+\omega_{f2}))(\hat{b}s^2+(\omega_f b-\hat{b}a)s-\omega_f b \hat{a})} y_M - \frac{s\hat{b}d}{\hat{b}s^2+(\omega_f b-\hat{b}a)s-\omega_f b \hat{a}} d \quad (\text{A.23})$$

When applying the final value theorem with a constant input signal the error converges to zero.

# Bibliography

- [1] Uwe Kiencke, Lars Nielsen  
Automotive Control Systems  
Springer-Verlag, Berlin Heidelberg, 2005
- [2] Manfred Burckhardt  
Radschlupf-Regelsysteme  
Vogel Verlag und Druck KG, Würzburg, 1993
- [3] Jens Kalkkuhl, Christian Urban  
Ein Erweitertes Kalmanfilter zur Seitenwinddetektion  
Technischer Bericht, DaimlerChrysler, 2005
- [4] A. Alcocer, A. Robertsson, A. Valera, R. Johansson  
Force Estimation and Control in Robot Manipulators  
Conference Paper, 7th Symposium on Robot Control, 2003
- [5] Karl J. Åström, Björn Wittenmark  
Computer Controlled Systems - 3rd ed.  
Prentice-Hall Inc., 1997
- [6] M. Mitschke, H. Wallentowitz  
Dynamik der Kraftfahrzeuge  
Springer, Berlin, 2004
- [7] Dieter Ammon  
Modellbildung und Systementwicklung in der Fahrzeugdynamik  
Teubner Verlag, 1997
- [8] Erich Schindler  
Vehicle Dynamics  
Lecture Notes, FHTE Esslingen, University of Applied Sciences
- [9] Michael Attinger  
Algorithmus zur Erkennung und Ausregelung von Fahrzeugreaktionen aufgrund von Straßenquerneigung  
Diplomarbeit, Institut für Flugmechanik und Flugregelung, Universität Stuttgart, 2005
- [10] Michael Pyper, Wilhelm Schiffer, Walter Schneider  
ABC - Active Body Control  
DaimlerChrysler, 2002